CANCER

The GAS6-AXL signaling network is a mesenchymal (Mes) molecular subtype–specific therapeutic target for ovarian cancer

Jane Antony,[1,2,3] Tuan Zea Tan,[1] Zoe Kelly,[3] Jeffrey Low,[4] Mahesh Choolani,[4] Chiara Recchi,[3] Hani Gabra,[3] Jean Paul Thiery,[1,5,6] Ruby Yun-Ju Huang[1,4,7]*

Ovarian cancer is a complex disease with heterogeneity among the gene expression molecular subtypes (GEMS) between patients. Patients with tumors of a mesenchymal ("Mes") subtype have a poorer prognosis than patients with tumors of an epithelial ("Epi") subtype. We evaluated GEMS of ovarian cancer patients for molecular signaling profiles and assessed how the differences in these profiles could be leveraged to improve patient clinical outcome. Kinome enrichment analysis identified AXL as a particularly abundant kinase in Mes-subtype tumor tissue and cell lines. In Mes cells, upon activation by its ligand GAS6, AXL coclustered with and transactivated the receptor tyrosine kinases (RTKs) cMET, EGFR, and HER2, producing sustained extracellular signal–regulated kinase (ERK) activation. In Epi-A cells, AXL was less abundant and induced a transient activation of ERK without evidence of RTK transactivation. AXL-RTK cross-talk also stimulated sustained activation of the transcription factor FRA1, which correlated with the induction of the epithelial-mesenchymal transition (EMT)–associated transcription factor SLUG and stimulation of motility exclusively in Mes-subtype cells. The AXL inhibitor R428 attenuated RTK and ERK activation and reduced cell motility in Mes cells in culture and reduced tumor growth in a chick chorioallantoic membrane model. A higher concentration of R428 was needed to inhibit ERK activation and cell motility in Epi-A cells. Silencing AXL in Mes-subtype cells reversed the mesenchymal phenotype in culture and abolished tumor formation in an orthotopic xenograft mouse model. Thus, AXL-targeted therapy may improve clinical outcome for patients with Mes-subtype ovarian cancer.

INTRODUCTION

Epithelial ovarian cancer is a lethal malignancy with nonspecific symptoms in early stages that enable silent progression of the disease. Most cases are diagnosed in the advanced stages, and despite treatment, prognosis is poor with 5-year survival lower than 30%. Locoregional dissemination of the tumor and metastases contribute to immense disease burden. Furthermore, epithelial ovarian cancer is hallmarked by a high degree of genetic and epigenetic aberrations, resulting in a diverse repertoire of modified cellular networks that can be delineated into distinct molecular subtypes based on gene expression profiling (*1*, *2*). These gene expression molecular subtypes (GEMS) are robust and reproducible as reported in the Australian Ovarian Cancer Study (*1*), The Cancer Genome Atlas (TCGA) (*2*), and by a large-scale meta-analysis study (*3*). At least five distinct GEMS of epithelial ovarian cancer have been identified: epithelial-A (Epi-A), epithelial-B (Epi-B), mesenchymal (Mes), Stem-A, and Stem-B (*3*). Elucidation of key signaling networks has further identified distinct players that promote tumorigenesis in each subtype.

The Stem-A subtype, which corresponds to the C5 subtype from the Tothill data set and the proliferative subtype from the TCGA data set, is driven by *MYCN* amplification (*4*) and *FZD7* overexpression (*5*), is enriched in microtubule-related gene sets, and is dependent on microtubule-associated genes for growth (*3*). The Mes subtype, which corresponds to the C1 subtype from the Tothill data set and the mesenchymal subtype from the TCGA data set, shows high correlation with transforming growth factor–β (TGF-β) pathway in gene set enrichment analysis (GSEA) with poor survival outcomes (*1*–*3*). The TGF-β pathway promotes epithelial-mesenchymal transition (EMT) (*6*). Mes-subtype tumors display extensive desmoplastic stromal reactions (*1*) that are associated with EMT and a microRNA network suppressing the expression of genes encoding E-cadherin (*CDH1*), vimentin (*VIM*), SLUG (*SNAI2*), and the epithelial transcriptional gatekeeper GRHL2 (*7*).

The RTK AXL belongs to the Tyro3-Axl-Mer (TAM) family of RTKs (*8*) along with MER and Tyro-3 and is activated by its ligand growth arrest–specific 6 (GAS6) (*9*). Its expression has been shown to be of prognostic value in breast (*10*) and lung (*11*) cancers. AXL has also been suggested as a therapeutic target for breast (*12*) and pancreatic cancer (*13*), and cancers demonstrating resistance to epidermal growth factor receptor (EGFR) and phosphatidylinositol 3-kinase (PI3K) inhibition (*14*–*16*). In epithelial ovarian cancer, *AXL* is highly expressed in advanced-stage diseases, predominantly in peritoneal deposits and metastases (*17*). Silencing *AXL* or blocking the GAS6-AXL pathway prevents regional dissemination of ovarian cancer cells in vivo (*18*). However, the role of AXL in the heterogeneous molecular backgrounds of epithelial ovarian cancer and the potential functional and therapeutic implication are yet to be defined.

The concept of GEMS-specific therapeutics has been well developed in breast cancer (*19*). However, data supporting the GEMS-specific management in epithelial ovarian cancer are newly emerging. The GEMS-specific pathways in epithelial ovarian cancer further point to the direction for developing new therapeutic strategies. The Stem-A subtype exhibits preferential sensitivity to microtubule destabilizers, such as vinorelbine (*3*). Inhibiting the TGF-β pathway might be a

[1]Cancer Science Institute of Singapore, National University of Singapore, Singapore 117599, Singapore. [2]NUS Graduate School for Integrative Sciences and Engineering, National University of Singapore, Singapore 117456, Singapore. [3]Department of Surgery and Cancer, Imperial College London, London W120NN, U.K. [4]Department of Obstetrics and Gynecology, National University Health System, Singapore 119228, Singapore. [5]Department of Biochemistry, Yong Loo Lin School of Medicine, National University of Singapore, Singapore 117596, Singapore. [6]Institute of Molecular and Cell Biology, A*STAR (Agency for Science, Technology and Research), Singapore 138673, Singapore. [7]Department of Anatomy, Yong Loo Lin School of Medicine, National University of Singapore, Singapore 117597, Singapore.
*Corresponding author. Email: ruby_yj_huang@nuhs.edu.sg

potential option for patients with the Mes subtype (*20*). The feasibility to stratify epithelial ovarian cancer patients on the basis of GEMS using a laboratory-based assay on formalin-fixed, paraffin-embedded (FFPE) diagnostic blocks has been demonstrated recently (*21*). Therefore, there is an eminent need in the field to quest for GEMS-specific therapeutic targets for epithelial ovarian cancer patients to achieve personalized precision management.

Here, we investigated the molecular differences in kinase signaling patterns among the various ovarian cancer GEMS and whether these profiles are predictive of therapeutic efficacy. Our data suggest that, in contrast to the Epi-A subtype, the Mes subtype is hallmarked by a receptor tyrosine kinase (RTK) cross-talk network sustained by the GAS6-AXL signaling node. The findings show how particularly the Mes and Epi-A subtypes differ, in molecular and cell behavior phenotypes as well as in drug response, thereby supporting the future development of GEMS-stratified clinical trials for epithelial ovarian cancer patients.

RESULTS

Interrogation of kinome profiles identifies *AXL* as highly expressed in Mes ovarian tumors and cell lines

Upon interrogating the kinome gene expression patterns in a published data set of ovarian cancer tumors and cell lines (*3*), we found that AXL was among the most highly expressed kinases in the Mes subtype (fig. S1, A and B). Tumors and cell lines of the Mes subtype in this data set (*3*) had significantly greater *AXL* gene expression than did the other subtypes (Fig. 1, A and B). Survival analysis showed that *AXL* overexpression correlated with poor prognosis in ovarian cancer patients (Fig. 1C) in both univariate and multivariate analyses (table S1). *AXL* was a prognostic factor for poor overall survival independent of known prognostic factors: patient age, tumor stage, tumor grade, and metastasis status. After stratification by the five GEMS, multivariate Cox's regression showed that *AXL* was still an independent prognostic factor for poor overall survival (table S2). The prognostic relevance of AXL has been validated in an independent cohort (fig. S1, C and D).

Mes, but not Stem-A, was largely positive for AXL when examining the total AXL protein expression in the SGOCL panel of ovarian cancer cell lines (*22*) matched with the GEMS (Fig. 1D) (*3*). Cells of the Epi-A and Epi-B subtypes collectively were moderately positive for AXL protein expression (Fig. 1D and fig. S1E). Because AXL has been associated with EMT, we further examined, within each GEMS, whether AXL expression would correlate with different phenotypes along the previously described EMT spectrum: epithelial (E), intermediate epithelial (IE), intermediate mesenchymal (IM), and mesenchymal (M) (*22*). Whereas the GEMS are principally delineated on the basis of molecular profiles, the EMT phenotypes are segregated on the basis of immunostaining and visualization of classic EMT markers such as E-cadherin, vimentin, and cytokeratins. From a phenotypic standpoint, cell lines of the IM phenotype, which has previously been shown to be an aggressive, anoikis-resistant state (*22*), were all positive for AXL abundance (Fig. 1D and fig. S1F) and also had the highest AXL abundance among the classifications (Fig. 1D and fig. S1G). AXL protein abundance was high in both Epi-A and Mes subtypes, whereas it was low in both Stem-A and Stem-B subtypes (Fig. 1D). These data suggest that although *AXL* is highly expressed in cells of the Mes and the IM phenotypes, it is also expressed abundantly in cells of the Epi-A and the IE phenotypes.

GEMS-specific AXL activation has divergent consequences in downstream ERK activation, cell proliferation, and motility

We next asked whether AXL played different roles in Mes and Epi-A. Cells representing the different ovarian cancer GEMS (fig. S2A) were stimulated with GAS6 over time to study the kinetics of downstream signaling by Western blotting for phosphorylated extracellular signal–regulated kinase (pERK) and pAKT responses. Upon GAS6-AXL activation, Mes showed two inductions of ERK phosphorylation at early (10, 20, and 30 min) and late (6 and 12 hours) time points (Fig. 1E and fig. S2C). The other subtypes, such as Epi-A and Stem-A, showed single induction of ERK activation only at the early time points (10, 20, and 30 min) (Fig. 1E and fig. S2C). Additional time course experiments showed that the pERK response in Epi-A subtype PEO1 cells is truly transient with no recurrence, whereas Mes-subtype SKOV3 cells showed multiple waves of ERK activation (fig. S2D). Within each GEMS, the EMT phenotypic classification further dictated the pattern of AKT activation (Fig. 1E and fig. S2, B and C). In GEMS with single inductions of pERK, such as Epi-A, Epi-B, and Stem-A subtype cells, AKT activation was induced once in cells of the epithelial or intermediate epithelial phenotype. However, in those of a mesenchymal or intermediate mesenchymal phenotype, AKT activation occurred in dual peaks (Fig. 1E and fig. S2, B and C). For Mes, AKT activation persisted from the early to the late time points regardless of the EMT phenotype (Fig. 1E and fig. S2, B and C). Densitometric quantitation further validated high abundance of pERK at both early and late time points in Mes, whereas Epi-A, Epi-B, and Stem-A showed pERK only at initial stages (Fig. 1F). Because changes in the temporal duration of ERK signaling elicit diverse biological outcomes (*23*, *24*), the recurrence of the pERK signal upon GAS6-AXL activation suggests that the temporal duration of the signal is sustained in Mes and that this might affect relevant downstream biological functions.

AXL signaling promotes cancer cell survival (*13*, *25*). A moderate increment in cell proliferation was observed upon GAS6 stimulation in all ovarian cancer GEMS without specific differences (fig. S2E). AXL signaling also enhances cancer cell invasion and metastasis (*13*, *26*). We utilized single-cell tracking to monitor cell motility by measuring several kinetic parameters such as displacement, velocity, speed, and directional persistence. Upon GAS6-AXL stimulation, Mes cells showed significant increase in all four kinetic parameters (fig. S2F). Upon GAS6 stimulation, Mes cell lines showed a significant enhancement in displacement (Fig. 1G and fig. S2G) and in gap closure migration assays (Fig. 1H and fig. S2H), whereas the other GEMS did not.

Together, GAS6-AXL activation has divergent control in downstream signaling and functions that are GEMS-specific in ovarian cancer. In Mes, it results in a recurrent sustained ERK response, which causes an increase in both proliferation and cell motility. However, in Epi-A, GAS6-AXL activation stimulates a single and transient ERK response that only results in an increase in proliferation.

GEMS-specific AXL activation reveals an extensive RTK cross-talk network in Mes

To understand the signaling circuitry that is connected to the recurrent ERK activation response specific to Mes-subtype cells, a reverse-phase protein array (RPPA) experiment was carried out using a Mes cell line (SKOV3) and an Epi-A cell line (PEO1) treated with GAS6 at 30 min and at 12 hours to evaluate the early and late responses, respectively. SKOV3 cells displayed increased abundance of pEGFR, pHER2, and pMET at both 30 min and 12 hours after GAS6 stimulation compared to the 0-min control (Fig. 2A). This pattern was

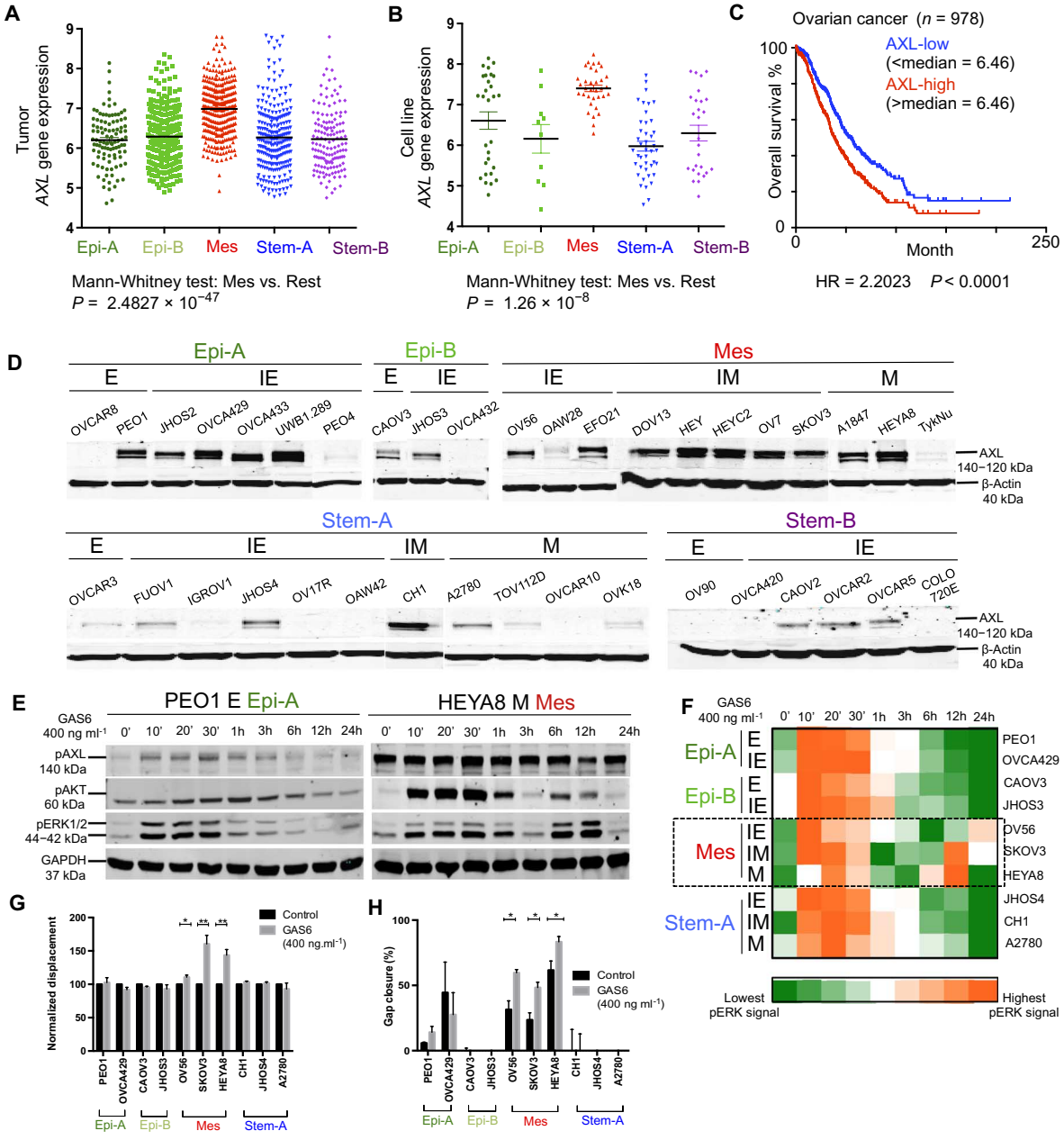

Fig. 1. The Mes subtype of ovarian cancer is enriched in *AXL* expression and shows recurrent ERK response and increased motility upon AXL activation. (**A**) *AXL* gene expression in 1538 ovarian tumor samples and 142 ovarian cell lines from a data set (*3*) classified into five distinct biological subtypes: Epi-A, Epi-B, Mes, Stem-A, and Stem-B. $P = 2.4827 \times 10^{-47}$ by Mann-Whitney test, Mes versus non-Mes. (**B**) As in (A) in subtype-associated cell lines ($P = 1.28 \times 10^{-8}$ by Mann-Whitney test, Mes versus rest). (**C**) Correlation of *AXL* expression with prognosis in ovarian cancer patients. Above median expression resulting in a hazard ratio (HR) of 2.2023. $P < 0.0001$ by log-rank test. (**D**) AXL protein abundance in a panel of ovarian cancer cell lines (SGOCL) assigned to the five subtypes. $P = 0.0138$, Mes versus non-Mes; $P = 0.0124$, Stem-A versus non-Stem-A; $P = 0.0871$, Epi-A versus non-Epi-A; $P = 0.892$, Epi-B versus non-Epi-B; $P = 0.1684$, Epi versus non-Epi; by Mann-Whitney tests. (**E**) Western blotting for pAXL, pAKT, and pERK in PEO1 (Epi-A) and HEYA8 (Mes) upon GAS6 stimulation for the indicated time points. Glyceraldehyde-3-phosphate dehydrogenase (GAPDH) was the loading control. (**F**) Heat map representing ERK response upon GAS6 stimulation of AXL in the 10 cell lines. (**G**) Displacement changes upon GAS6 activation of AXL in epithelial ovarian cancer subtypes. (**H**) Gap closure rates upon GAS6 stimulation in epithelial ovarian cancer subtypes. Data in (E) to (H) are means ± SEM from at least three experiments; *$P < 0.05$, **$P < 0.01$, and ***$P < 0.001$ by Student's *t* tests. Blots are representative of three experiments.

parallel to the higher and sustained pAXL signals observed previously by Western blotting (Fig. 1E and fig. S2C). This suggested that there were cross-talks between AXL and other RTKs in Mes. However, this RTK cross-talk phenomenon was completely deficient in the Epi-A PEO1 system, where no significant transactivation of EGFR, HER2, or cMET was detected after GAS6 treatment (Fig. 2A). The RPPA results were validated by Western blotting and extended to the cell lines OVCA429 (Epi-A) and HEYA8 (Mes) (Fig. 2B). An in situ proximity ligation assay, Duolink, was carried out to explore whether the cross-talks between AXL and these RTKs were mediated via protein-protein

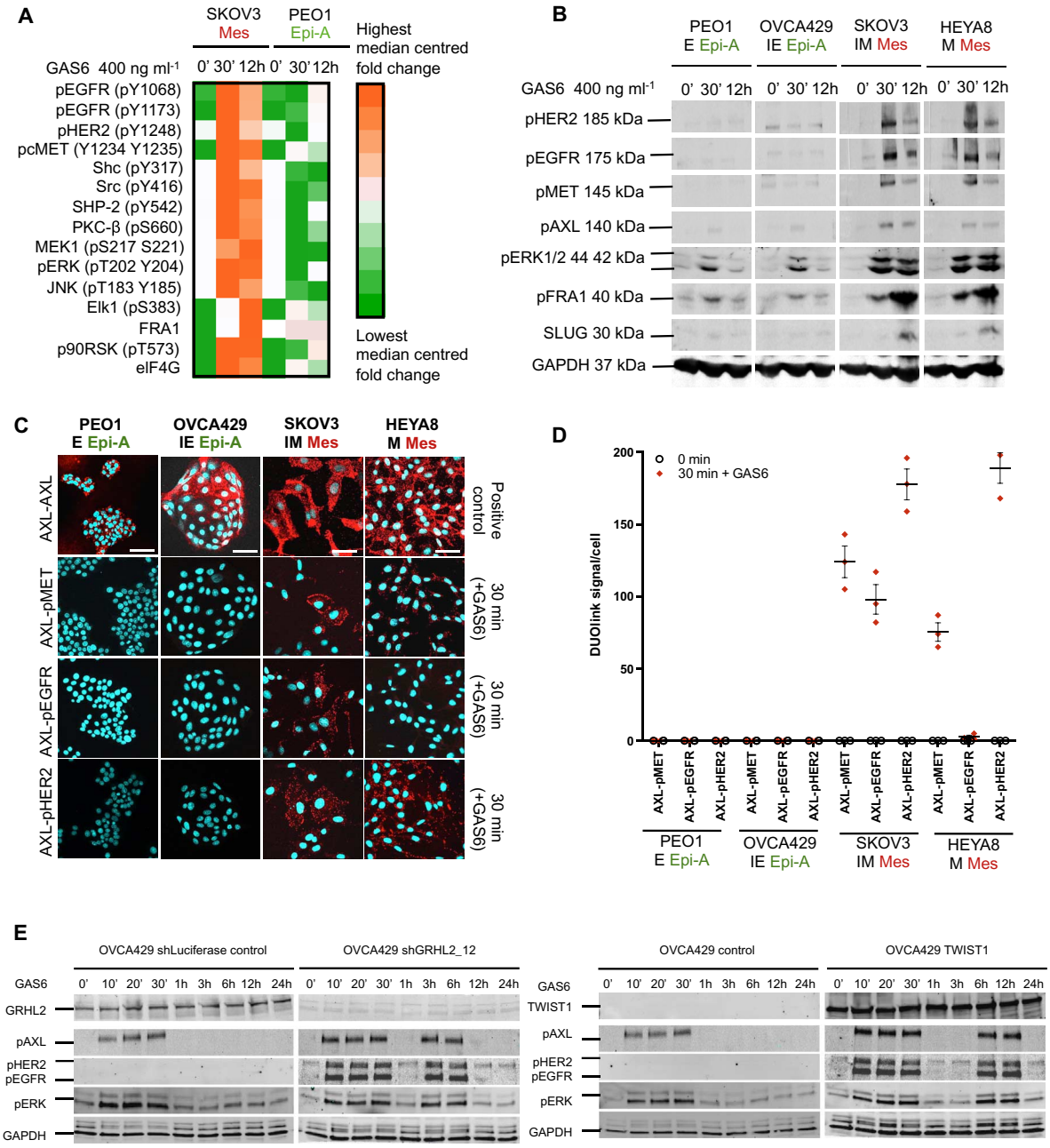

Fig. 2. AXL is enmeshed in an RTK network in the Mes subtype. (**A**) RPPA depicting global proteomic and phosphoproteomic changes upon AXL stimulation by GAS6. (**B**) Western blotting or phosphorylated RTKs and downstream signaling moieties in epithelial ovarian cancer cell lines PEO1 and OVCA429 (Epi-A) and SKOV3 and HEYA8 (Mes) upon AXL activation. (**C**) Proximity ligation assay showing the extent of interactions of pMET, pHER2, and pEGFR with AXL upon activation with GAS6 in SKOV3 and HEYA8 (Mes) or PEO1 and OVCA429 (Epi-A) cells. As a positive control, AXL-AXL interaction was assessed with two different antibodies targeting the C terminus and N terminus of AXL. Scale bars, 50 μm. (**D**) Quantification of Duolink signals in (C) using ImageJ. Data are means ± SEM from at least three experiments; *$P < 0.05$, **$P < 0.01$, and ***$P < 0.001$ by Student's t tests. (**E**) Western blotting for pAXL, pEGFR, pHER2, and pERK in GAS6-stimulated OVCA429 cells, transfected with GRHL2 short hairpin–mediated RNA (shRNA), TWIST1, or the corresponding control. Blots and microscopy images are representative of three experiments.

interactions. Upon GAS6 stimulation in Mes cell lines SKOV3 and HEYA8, Duolink showed signals for interactions between AXL and the phosphorylated forms of the RTKs Met, HER2 and EGFR (Fig. 2, C and D). This transactivation was not seen at the resting state when GAS6 is absent (fig. S3A). This indicated that ligand-activated AXL might trigger the phosphorylation of other RTKs through receptor clustering. This phenomenon of AXL-RTK clustering was not observed in Epi-A lines PEO1 and OVCA429 (Fig. 2, C and D). The difference in transactivation was not due to the expression status of the RTKs since all chosen cell lines were positive for cMET, HER2, and EGFR expression (fig. S3B).

Downstream of the RTK network, adapter proteins such as SHC, SRC, and SHP2 and the mitogen-activated protein kinase (MAPK) pathway kinases MEK1, ERK, and JNK had increased phosphorylation

upon GAS6 stimulation in SKOV3 but not in PEO1 cells (Fig. 2A). Their activation correlated with the phosphorylation of sustained response proteins such as ELK1, p90RSK, and FRA1 at 12 hours in SKOV3 cells, which was absent in PEO1 cells (Fig. 2A). FRA1 induction alongside the sustained ERK activation was confirmed by Western blot analysis (Fig. 2B). Sustained activation of ERK stabilizes FRA1 (*27*), the activity of which has been linked to the induction of EMT transcription factors ZEB1 and SLUG and, consequently, increased motility (*28*). SLUG induction in Mes was confirmed by Western blotting (Fig. 2B). The MEK inhibitor PD0325901 (*29*) prevented phosphorylation of the MEK-ERK axis in Epi-A and Mes and consequently prevented induction of FRA1 and SLUG in Mes (fig. S3C). Furthermore, MEK inhibition prevented GAS6-AXL–mediated motility induction in Mes (fig. S3, D to G), suggesting that AXL signaling relies on the MEK-ERK cascade to induce motility. Furthermore, the ERK inhibitor SCH772984 (*30*) prevented the induction of pERK in a time course–dependent manner (fig. S3, H and I).

Together, our data indicate that the AXL-RTK network and the signaling cascade responsible for the increased cell motility in Mes are deficient in other GEMS, such as Epi-A. The Mes subtype is wired with a unique signaling cross-talk network that contributes to its biological functions. Indeed, knocking down epithelial status maintaining transcription factor GRHL2 (*7*) or overexpressing EMT inducing TWIST1 (*31*) in epithelial OVCA429 promoted a mesenchymal phenotype (fig. S3J) and induced AXL-RTK cross-talk and recurrent pERK response (Fig. 2E).

AXL kinase domain is crucial to initiate phosphorylation of RTKs

To study the functional relevance of the AXL kinase domian, we transfected *AXL*-null Epi-A cell line PEO4, and Mes cell line TYKnu with a plasmid encoding either functional AXL or a kinase-deficient K567R mutant AXL (Fig. 3A) (*32*). Stimulation of AXL-transfected PEO4 cells with GAS6 for 30 min induced the phosphorylation of AXL but not EGFR, as expected of epithelial systems (Fig. 3B). Stimulation of transfected TYKnu cells with GAS6 induces the phosphorylation of AXL as well as EGFR. However, in AXL^{K567R} (kinase-deficient)–transfected TYKnu cells, neither AXL nor EGFR was activated (Fig. 3B). Duolink assays were carried out to corroborate these Western blot results and investigate the interaction between AXL and EGFR. AXL-EGFR clustering occurred in both AXL- and AXL^{K567R}-transfected Mes-subtype TYKnu cells; however, no pEGFR was detected in AXL^{K567R}-transfected cells (Fig. 3C). This suggests that GAS6-AXL signaling–induced RTK cross-talk relies on the AXL kinase activity to phosphorylate the other RTKs.

Epithelial systems are under dual regulation of membrane rafts and cellular phosphatases to curtail AXL signaling

To decipher the differential modulation of AXL signaling in Epi and Mes systems, we investigated the role of membrane-organized lipid rafts, which regulate signal transduction (*33*). We depleted cholesterol, an integral component of the lipid rafts, using methyl-β-cyclodextrin (MBCD) in Epi-A cell lines PEO1 and OVCA429 and Mes cell lines SKOV3 and HEYA8. Cholesterol depletion, as measured by the intensity of cholesterol-bound filipin staining, was observed up to 12 hours after MBCD treatment (Fig. 4A). Subsequent to loss of membrane architecture integrity, GAS6 stimulation resulted in AXL-RTK cross-talk in Epi-A subtype PEO1 and OVCA429 at early (30 min) and late

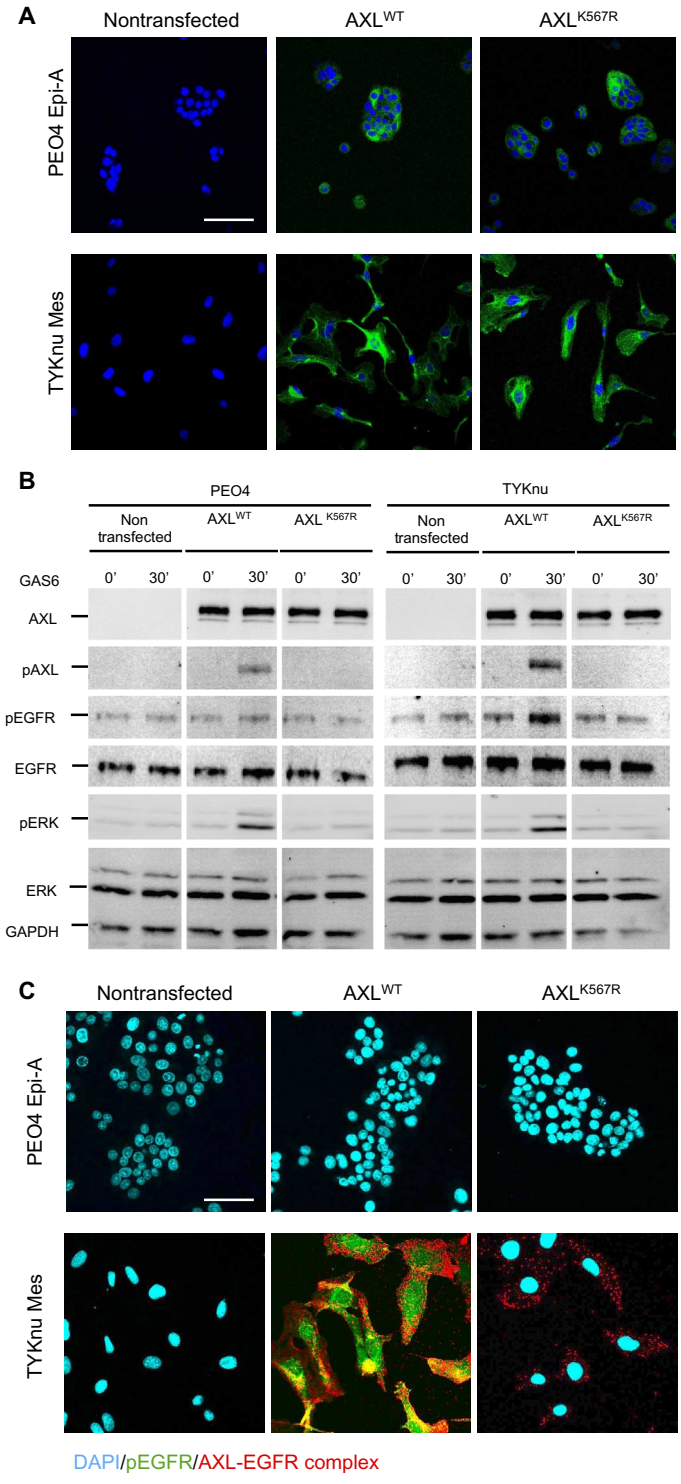

Fig. 3. AXL kinase domain is crucial for phosphorylation of other RTKs. (**A**) Immunostaining of AXL-deficient Epi-A subtype PEO4 cells and Mes-subtype TYKnu cells, transfected with wild-type AXL (AXL^{WT}) or AXL^{K567R}. (**B**) Western blotting for pAXL, pEGFR, and pERK in Mes TYKnu and in Epi-A PEO1 cells transfected with AXL^{WT} or AXL^{K567R} and stimulated with GAS6. (**C**) Proximity ligation assay to assess AXL-EGFR cross-talk (red dots) upon stimulation with GAS6 in Mes TYKnu and in Epi-A PEO4 cells transfected with AXL^{WT} or AXL^{K567R}, alongside immunostaining for pEGFR (green). Scale bars, 50 μm. Blots and microscopy images are representative of three experiments.

(12 hours) time points but only induced ERK activation at the early time point (Fig. 4B). This suggested that epithelial systems are under modulation of more than just the membrane rafts. To investigate the cause of the reduced ERK response, even upon increased AXL-RTK cross-talk, we analyzed the expression pattern of dual specificity phosphatases (DUSPs) across the Epi-A and Mes subtypes (Fig. 4C). DUSP4, with an abundance significantly lower in Mes subtype (Fig. 4D), dephosphorylates ERK to modulate the MEK-ERK cascade in ovarian cancer (*34*). Silencing DUSP4 with small interfering RNA (siRNA) in Epi-A PEO1 and OVCA429 cells (Fig. 4E) increased the temporal ERK response (Fig. 4F and fig. S4A) but not to the extent that was observed in Mes cells. This may be explained by lack of AXL-RTK cross-talk in Epi-A cells. Epi-A cells treated with both MBCD and DUSP4 siRNA induced AXL-RTK cross-talk as well as ERK activation at a later time point (Fig. 4G and fig. S4B). In epithelial systems, RTK networks are modulated by membrane architecture, and ERK activity is regulated by DUSP4; thus, loss of both these regulatory mechanisms enables a signaling phenotype that is mesenchymal-like (Fig. 4H).

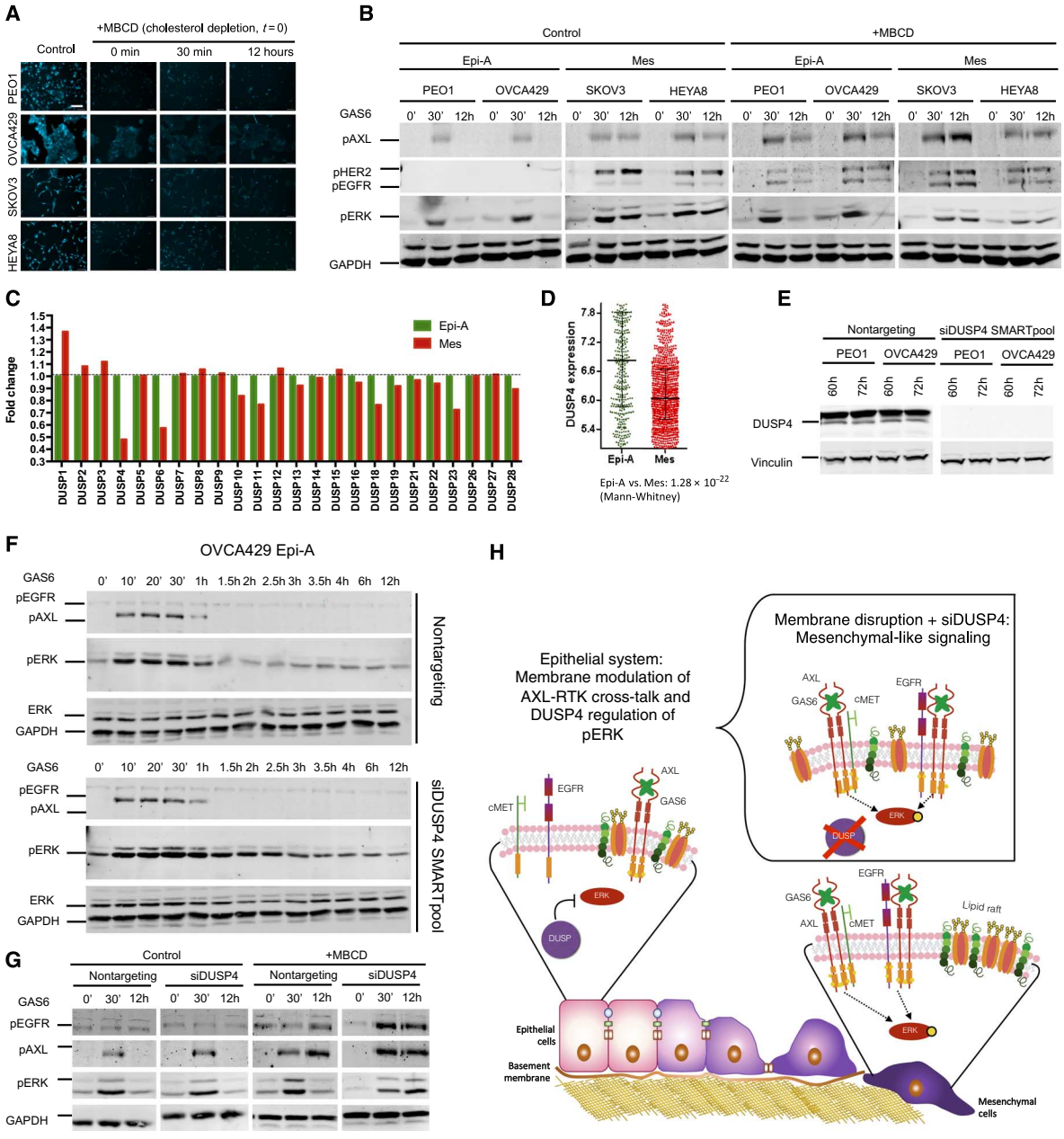

Fig. 4. Membrane rafts and cellular phosphatases regulate epithelial systems to downmodulate AXL signaling. (**A**) Cholesterol, visualized by filipin staining, in cells cultured with MBCD for up to 12 hours. Scale bar, 200 μm. (**B**) Western blotting for AXL-RTK cross-talk and pERK in Epi-A–subtype PEO1 and OVCA429 upon stimulation with GAS6. (**C**) Expression of the DUSPs from the gene expression database CSIOVDB (*38*). (**D**) DUSP4 expression in Epi-A compared with Mes subtypes. $P = 1.28 \times 10^{-}22$ by Mann-Whitney test. (**E**) DUSP4 knockdown using a DUSP4-targeting SMARTpool siRNA compared to a control siRNA in PEO1 and OVCA429 cells. (**F**) Western blotting for pERK response upon GAS6 stimulation in DUSP4-depleted or control OVCA429 cells. (**G**) Western blotting for pERK and RTK cross-talk in DUSP4- and cholesterol-depleted OVCA429 cells upon GAS6 stimulation. (**H**) Schematic overview of AXL signaling and modulation. Blots and microscopy images are representative of three experiments.

The Mes subtype is more sensitive to the AXL inhibitor R428

R428, an AXL-selective inhibitor, blocks tumor dissemination and prolongs survival in mouse models of metastatic breast cancer (*12*). To support specificity of the inhibitor, we first confirmed that R428 did not disrupt EGF-EGFR signaling (fig. S5A). To test whether R428 causes different effects among ovarian cancer GEMS, we treated 10 selected cell lines representing the different GEMS (fig. S2A) with R428 for 48 hours to determine the 50% growth inhibition (GI_{50}) concentrations. Mes cell lines had a significantly lower mean GI_{50} of 2.91 μM compared to the other subtypes with a mean GI_{50} of 9.38 μM (P = 0.016) (Fig. 5A). Furthermore, AXL-deficient Epi-A PEO4 cells, and Mes TYKnu cells, were transfected with wild-type or kinase-deficient (K567R) AXL and treated with R428. The R428-mediated GI_{50} in AXL-null PEO4 and TYKnu cells was high at 195.9 and 262.86 μM, respectively, enforcing the specificity of the AXL inhibitor (fig. S5B). High GI_{50} was also observed in kinase-deficient AXL^{K567R}-transfected PEO4 cells (276.6 μM) and TYKnu cells (245.5 μM), confirming the

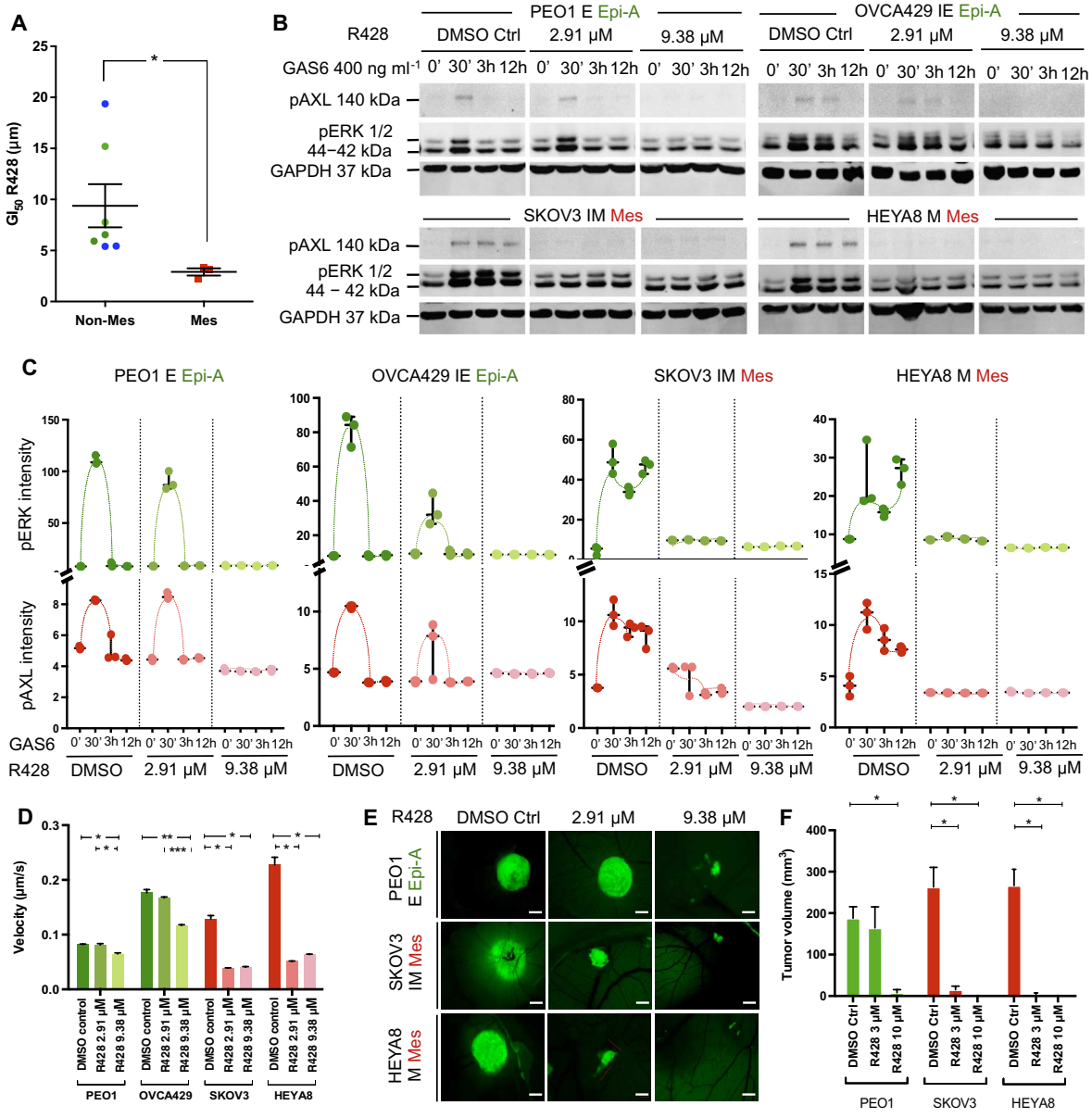

Fig. 5. The Mes subtype is more sensitive to the AXL inhibitor R428. (**A**) GI_{50} values for AXL inhibitor R428 in epithelial ovarian cancer cell lines. P = 0.0167, Mes versus non-Mes by Mann-Whitney test. (**B**) Western blotting for pAXL, pAKT, and pERK in epithelial ovarian cancer cell lines PEO1 and OVCA429 (Epi-A) or SKOV3 and HEYA8 (Mes), preincubated with DMSO [control (Ctrl)], 2.91 μM R428 (GI_{50}^{Mes}), or 9.38 μM R428 ($GI_{50}^{non\text{-}Mes}$) for an hour, then stimulated with GAS6 for 0.5, 3, or 12 hours. (**C**) Quantitation of immunofluorescence staining for pAXL, pAKT, and pERK in epithelial ovarian cancer cell lines PEO1 and OVCA429 (Epi-A) or SKOV3 and HEYA8 (Mes) upon treatment with the indicated dose of R428. (**D**) Velocity of Epi-A– and Mes-subtype cell lines exposed to 2.91 μM (GI_{50}^{Mes}) or 9.38 μM R428 ($GI_{50}^{non\text{-}Mes}$). (**E**) Chick CAM model of Mes or Epi-A cell line tumor growth in response to R428. Scale bars, 2000 μm. (**F**) Tumor volume as the mean radius (r) of the fluorescent tumor was calculated relative to background. Tumor was assumed to be a spheroid with volume $4\pi r^3/3$. Data in (A), (C), (D), and (F) are means ± SEM from at least three experiments; *P < 0.05, **P < 0.01, and ***P < 0.001 by Student's t tests. Blots and microscopy images are representative of three experiments.

relevance of the AXL kinase domain (fig. S5B). Transfections with functional wild-type AXL showed a GI_{50} of 30.48 μM in Epi-A PEO4 cells and a significantly lower GI_{50} of 3.45 μM in Mes TYKnu cells (fig. S5B).

Because Mes has a unique GAS6-AXL signaling network, we explored the effect of R428 on this signaling network in comparison to Epi-A. Two Epi-A lines (PEO1 and OVCA429) and two Mes lines (SKOV3 and HEYA8) were chosen and preincubated with dimethyl sulfoxide (DMSO; control), 2.91 μM (GI_{50}^{Mes}), and 9.38 μM ($GI_{50}^{non\text{-}Mes}$) of R428. From both Western blotting and immunostaining, the early-phase ERK activation in Epi-A was only inhibited at the higher concentration of R428 at 9.38 μM, whereas the early- and late-phase ERK activation in Mes were effectively inhibited at the lower concentration of 2.91 μM (Fig. 5, B and C, and fig. S5C). In addition, these four cell lines also represent different phenotypes along the EMT spectrum (E, PEO1; IE, OVCA429; IM, SKOV3; M, HEYA8). From the phenotypic perspective, lower R428 concentration of 2.91 μM had no effect on the pERK and pAXL activations in PEO1 (E), whereas OVCA429 (IE) showed a moderate reduction (Fig. 5C and fig. S5C). The SKOV3 (IM) line showed a drastic decrease, whereas the HEYA8 (M) line showed complete inhibition at 2.91 μM (Fig. 5C and fig. S5C). Mes shows dependence on the GAS6-AXL axis and is therefore very sensitive to AXL inhibition. In addition, complex RTK networks connected by AXL might govern the phenotypic transition along the EMT gradient.

To analyze the functional consequences following AXL signaling inhibition, we preincubated PEO1, OVCA429, SKOV3, and HEYA8 with R428 and tracked for motility. Similar to the pERK and pAXL signaling inhibition, Epi-A cell lines showed motility inhibition only at the higher concentration of R428, whereas Mes cell lines showed effective inhibition at the lower concentration (Fig. 5D and fig. S5, D to F).

To translate the AXL signaling inhibition and functional repression to a biologically relevant system, we embedded the four cell lines in Matrigel and deposited on top of the chick chorioallantoic membrane (CAM) model to study the relevance of AXL inhibition in ovo. The in ovo findings substantiated the in vitro results, with HEYA8 and SKOV3 forming large tumors in the CAM, which were significantly suppressed at 2.91 μM as well as at 9.38 μM of R428 (Fig. 5, E and F). Unlike its Mes counterparts, tumor formation in PEO1 was not inhibited at 2.91 μM but only at 9.38 μM (Fig. 5, E and F). The OVCA429 line proved to be nontumorigenic in the CAM system. Together, these results indicated the preferential application of inhibiting AXL in the Mes subtype of epithelial ovarian cancer, in which significant sensitization to R428 can be achieved.

AXL governs the sequential phenotypic and functional transition of EMT

Apart from pharmacological inhibition of AXL, shRNA-mediated silencing of AXL was also utilized to better understand its functional role in ovarian cancer. Two shRNAs (shAXL#40 and shAXL#41) were used to knock down AXL, and a nontargeting shRNA (shLuciferase) was used as a control, in Epi-A OVCA429 and Mes SKOV3 cell lines. More than 90% reduction in total AXL protein expression was achieved by both shRNAs (Fig. 6A). Phase-contrast images revealed that in shAXL clones, OVCA429 formed more compact colonies, and SKOV3 reverted from a fibroblastic to a loosely defined colony structure (Fig. 6B). Immunofluorescence staining revealed that shAXL OVCA429 cells increased the intensity of E-cadherin staining at the cell-cell junctions together with a complete restoration of cytoplasmic β-catenin to the junctions (Fig. 6C). The shAXL SKOV3 cells showed reexpression of E-cadherin, which was mostly cytoplasmic with partial restoration to the cell-cell junctions (Fig. 6C). These data suggested that AXL knockdown causes a partial reversal along the EMT spectrum. The reversal in OVCA429 is from an IE state to a more epithelial state, whereas the SKOV3 reverts from an IM state to an IE state. This implies that the extent of EMT reversal upon AXL knockdown is sequential and depends on the cell line's original EMT state (Fig. 6D). Note that although the Mes subtype is indeed more sensitive to pharmacological inhibition of AXL at lower doses of R428, shRNA-mediated AXL silencing did not induce differential survival benefits but induced EMT reversal in both Epi-A and Mes.

To substantiate the functional effect of partial EMT reversal in shAXL cells, we carried out motility assays. Single-cell motility analysis and gap closure assays in shAXL#40 and shAXL#41 clones showed a significant reduction (fig. S6, A to C). These results were consistent with the functional changes in cell motility after R428 inhibition.

AXL knockdown reduces anchorage-independent growth, invasion, and tumor formation

In addition to the effect on EMT reversal, proliferation, soft agar, and invasion assays were carried out in the shAXL cells. Both Mes SKOV3 and Epi-A OVCA429 shAXL cell lines showed reduced proliferation (Fig. 6, E and F). This is concordant with the proliferative effects observed after GAS6 stimulation that both Epi-A and Mes require AXL signaling for cell growth. For soft agar assays, OVCA429 cells showed minimal colony formation, which was completely abrogated in shAXL (Fig. 6G and fig. S6D). In SKOV3, the control cells showed significant colony formation in soft agar, and shAXL attenuated its clonogenic ability (Fig. 6G and fig. S6D). Spheroid invasion assays showed a similar trend with OVCA429, forming minimally invasive spheroids, an effect that was completely prevented in shAXL. SKOV3 showed numerous invasive protrusions from the spheroids, which was abolished in shAXL (Fig. 6H and fig. S6E).

When the spheroid invasion assay was performed in reduced serum conditions with GAS6 treatment, only the Mes SKOV3 cell line showed invasion, but not the Epi-A OVCA429 cell line (fig. S6, F and G). Our data suggested that AXL played an important role in both the anchorage-dependent and anchorage-independent growth. It is particularly essential for the mesenchymal phenotype such as Mes that AXL is required for anchorage independency.

In an orthotopic xenograft tumor model in mice, shAXL#40 and shAXL#41 SKOV3 cells showed complete inhibition of tumor formation and growth compared to shLuciferase control. Tumor inhibition was 100%, with SKOV3 shLuciferase control forming tumors [average weight of 0.3658 g (SEM, 0.1563); average number of 5.8 (SEM, 0.74)], and the SKOV3 shAXL#40 and shAXL#41 clones forming no tumors ($P = 0.0474$; $P = 0.0001$) (Fig. 6, I and J). This is consistent with the R428-mediated tumor reduction observed in the in ovo CAM model, suggesting that AXL is indeed a key signaling node for Mes.

The *AXL* signature is clinically relevant for patient stratification

A gene signature of the top 30 genes correlating with *AXL* expression (Fig. 7A) was derived from the gene expression microarray analysis (*3*). This "AXL gene signature" was significantly overexpressed in Mes-type tumors (Fig. 7B). EMT scoring is a quantitative measure of the effects of EMT on cancer progression (*35*); GEMS classification and EMT status in ovarian tumors robustly correlate with a poor

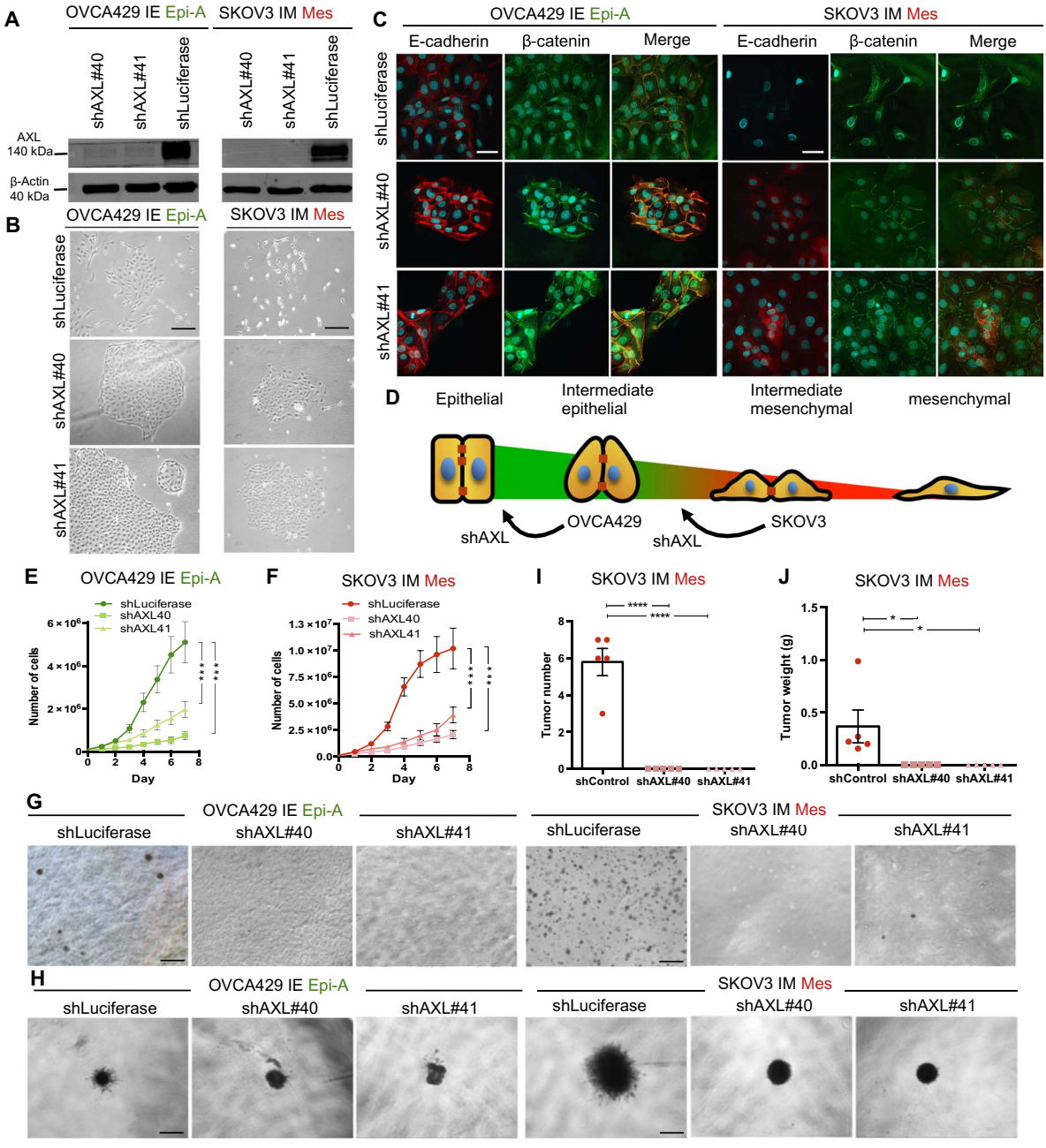

Fig. 6. AXL governs the sequential phenotypic and functional transition of EMT. (**A**) Western blotting of AXL in OVCA429 and SKOV3 cells upon transfection with one of the two AXL shRNAs or a control (shLuciferase). (**B**) Phase-contrast images showing colony formation phenotype upon AXL knockdown in OVCA429 and SKOV3 cells. Scale bars, 200 μm. (**C**) Immunostaining for E-cadherin and β-catenin abundance and localization in OVCA429 and SKOV3 cells upon AXL knockdown. Scale bars, 50 μm. (**D**) Schematic of partial EMT reversal facilitated by AXL knockdown, from an "intermediate mesenchymal" to an "intermediate epithelial" state in SKOV3 cells, and from an "intermediate epithelial" state to a more "epithelial" state in OVCA429 cells. (**E** and **F**) Proliferation in cultured SKOV3 (E) and OVCA429 (F) cells upon AXL knockdown. (**G**) Colony formation in soft agar in SKOV3 and OVCA429 cell lines upon AXL knockdown. Scale bars, 200 μm. (**H**) Spheroid invasion in complete medium in SKOV3 and OVCA429 cell lines upon AXL knockdown. Scale bars, 200 μm. (**I** and **J**) Tumor number (I) and mass (J) in severe combined immunodeficient (SCID)–Beige mice 4 weeks after intraperitoneal injection with SKOV3 cells (5×10^6 cells, 200 μl of suspension) transfected with either shLuciferase (control) or one of two AXL shRNAs. Data are means ± SEM from at least three experiments (E and F) or five mice per condition (I and J); $^*P < 0.05$, $^{**}P < 0.01$, $^{***}P < 0.001$, and $^{****}P < 0.0001$ by Student's *t* tests. Blots and microscopy images are representative of 3 experiments.

prognosis in patients (*35*). By analyzing the gene expression profiling meta-analysis cohort (*3*), the AXL gene signature positively correlated with the ovarian-specific EMT score (Rho = +0.4148, $P = 5.23 \times 10^{-65}$) (Fig. 7C) and negatively correlated with overall patient survival (Fig. 7D). These findings were validated in an independent cohort (fig. S7, A to C). Multivariate analysis also shows a significant prognostic relevance of the *AXL* signature (table S3). In addition, the AXL gene signature was significantly overexpressed in omental metastases (*36*) ($P = 0.0078$) and platinum-resistant relapsed tumors (*37*) ($P = 0.0059$) compared to their paired primary tumors (Fig. 7E). This is

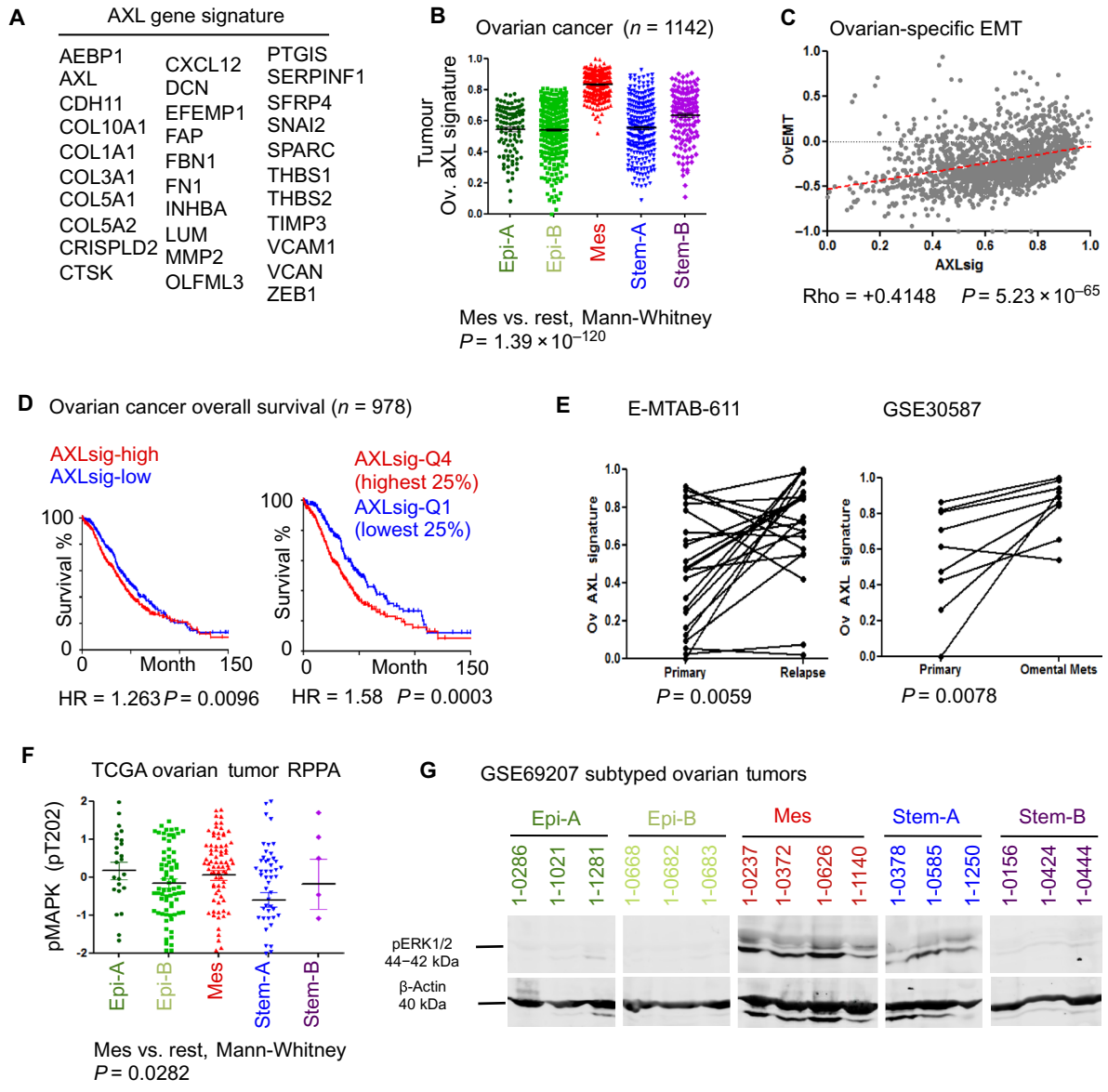

Fig. 7. *AXL* signature positively correlates with EMT and confers worse prognosis. (**A**) AXL gene signature, defined by the cluster of genes that positively correlated with *AXL* expression in a published microarray (*3*). (**B**) Expression pattern of the AXL gene signature in ovarian tumor samples [$n = 1142$ (*3*)] classified by ovarian GEMS. $P = 1.39 \times 10^{-120}$ by Mann-Whitney test, Mes versus the rest. Ov., ovarian. (**C**) Correlation of AXL gene signature with ovarian-specific EMT score in tumor samples (*3*). Rho = +0.4148; $P = 5.23 \times 10^{-65}$. (**D**) Survival in ovarian cancer patients (*3*) classified by expression of the AXL gene signature (AXLsig) and analyzed either by median expression (left) or by the lowest and highest quadrants (right). (**E**) AXL signature in platinum-resistant relapsed tumors from the E-MTAB-611 data set (left; $P = 0.0059$) and in omental metastases from the GSE30587 data set (right; $P = 0.0078$), each compared to the paired primary tumor. (**F**) RPPA-based abundance of pMAPK (pThr^{202}) in Mes subtype ovarian tumors from the TCGA, $P = 0.0282$ by Mann-Whitney test, Mes versus the rest. (**G**) Western blotting for pERK1 (Thr^{202}/Tyr^{204}) and phosphorylated (Thr^{185}/Tyr^{187}) ERK2 in epithelial ovarian cancer tumor samples classified by subtype.

consistent with the notion that AXL overexpression is associated with poor prognosis (*26*). The strong correlation between AXL and EMT further highlighted its relevance in EMT modulation and subsequent effects in promoting tumor dissemination and drug resistance, which translates to patient survival. Analyzing RPPA data in the TCGA revealed greater abundance of pMAPK in Mes-subtype cells ($P = 0.0282$) (Fig. 7F); we propose that this could at least partially be the result of increased GAS6-AXL signaling and RTK cross-talk. An increased phosphorylation of ERK in Mes-type cells was validated by Western blotting tumor samples that had been previously stratified by GEMS (Fig. 7G) (*38*).

Together, our data indicate that cells of different GEMS in ovarian cancer show varied responses to the same kinase signaling axis that direct functional and therapeutic consequences. In particular, our data suggest that the Mes subtype is addicted to the GAS6-AXL-RTK cross-talk. The recurrent temporal activation of ERK downstream to GAS6-AXL results functionally in a motile and invasive phenotype that is synonymous with EMT. Therapeutically, the amplified signaling sensitizes the Mes subtype to AXL inhibition, thus providing evidence to utilize AXL as a GEMS-specific target. Moreover, because our data indicate that AXL mediates EMT, stratifying patients for AXL inhibition on the basis of EMT status may also be a rational clinical strategy.

DISCUSSION

AXL was originally identified as a transforming gene in human myeloid leukemia cells (*39*). There is ectopic expression or overexpression in several cancers including glioblastoma, lung, breast, colorectal, gastric, pancreatic, bladder, renal, endometrial, and ovarian cancer (*17*). In ovarian cancer, AXL is crucial to initiate and sustain metastasis and tumor dissemination in mouse models (*18*). However, given the vast molecular heterogeneity of the disease, the biology of AXL in the ovarian context is unclear. Here, we illustrated the divergent roles of AXL among the GEMS in ovarian cancer. AXL is significantly enriched in Mes, and its activation potentiates cross-talk with EGFR and cMET, amplifying downstream oncogenic signaling such as recurrent pERK peaks. The differential pERK responses between Epi-A and Mes could potentially be linked to an increased complex network of RTK interactions along the EMT spectrum, resulting in the amplification of RTK signaling. Our results indicate a reliance of the Mes subtype on the GAS6-AXL module to propagate RTK signaling interactions. AXL has been previously shown to interact with cMET (*40*), EGFR (*14*), and HER2 (*41*) in lung and breast cancers. In head and neck and esophageal squamous cell carcinomas, it has been reported that AXL dimerizes with EGFR to confer resistance to PI3K inhibition (*16*). This AXL-RTK cross-talk might exist in reciprocal control since activation of EGFR was shown to transactivate AXL in triple-negative breast cancer, thereby promoting additional signaling cascades to effect motility responses (*42*). Notably, inhibiting AXL in MCF7 and T47D cell lines had no effect, whereas the MDA-MB-231 and MDA-MB-157 showed loss of EGFR-mediated functions when AXL was inhibited (*42*). The former two cell lines have a negative EMT score and are classified as epithelial, whereas the latter have a positive EMT score and are classified as mesenchymal (*35*). Therefore, this AXL-RTK reciprocal cross-talk might be tightly governed by the intrinsic EMT status that only exists in the mesenchymal phenotype. This alludes to the conserved ability of one oncogenic RTK to recruit and activate other receptors through clustering, leading to the diversification of signaling pathways in cells that have undergone an EMT, conferring the mesenchymal state with a more aggressive phenotype. Additional evidence comes from targeting AXL with a high-affinity RNA-based inhibitory aptamer GL21.T that abrogates AXL-mediated invasion and tumor growth in mice (*43*). This aptamer selectively accumulates in the AXL-overexpressing, mesenchymal-like A549 xenograft (*43*) but not in the AXL-low, epithelial MCF7. In mesenchymal systems such as A459 and MDA-MB-231, AXL inhibition improves responses to erlotinib and reduces metastasis in vivo (*44*). Collectively, it is clear that anti-AXL therapy will principally be efficacious in systems that have undergone EMT. However, it is worthwhile to note that in pancreatic cancer models in mice, anti-AXL monoclonal antibodies (mAbs) have inhibited the growth of xenografts derived from epithelial cell lines (such as BxPC-3) and mesenchymal cell lines (such as MiaPaCa-2) alike (*45*).

Downstream the AXL-RTK network, several adapter proteins such as SHC, SRC, and SHP-2 are activated in Mes but not in Epi-A. This is paralleled to the recurrent ERK activation followed by FRA1 induction. Consequently, the sustained ERK and FRA1 activation contributes to an EMT-like phenotype in terms of enhanced motility. ERK activation has been previously linked to motility (*46*) via the EMT-inducing transcription factor Slug (*47*). The ERK/FRA1 axis is involved in modulating the EMT transcription factors Slug and ZEB1 and cell motility (*27*, *48*). Our data not only corroborate with these findings but also provide additional significance in the specific activation of this signaling cascade in a clinically relevant subset of ovarian cancer, the Mes subtype. This might lead to a targetable conduit for the AXL-RTK-ERK axis by precise patient stratification in ovarian cancer. The tendency of Mes to amplify AXL signaling results into an increase in the sensitivity to pharmacological inhibition of AXL compared to other ovarian cancer GEMS. In lung cancer, mesenchymal cells are more sensitive to AXL inhibition by the small-molecule inhibitor SGI-7079, and this is primarily because of increased AXL abundance (*15*). However, our findings further show that in addition to AXL abundance, the AXL-RTK-ERK cross-talk pattern is another important feature to determine the sensitivity to AXL inhibition.

AXL-associated EMT has been shown to mediate resistance to targeted therapy (*12*, *14*, *15*, *49*, *50*). Pharmacologic inhibition of AXL activity has been demonstrated to reverse the resistance. In non–small cell lung cancer, mesenchymal cells show greater resistance to EGFR-targeted therapy due to increased abundance of AXL. This resistance can be reversed by inhibiting AXL (*15*), which suggests oncogenic dependence on AXL in systems that have undergone EMT. Increased activation of AXL in the absence of acquired EGFR T790M mutation or cMET activation confers erlotinib resistance in multiple lung cancer models in vitro and in vivo, with genetic or pharmacologic inhibition of AXL restoring sensitivity (*14*). These findings highlight the therapeutic potential of AXL inhibition in drug-resistant tumors. Currently, there are several AXL-targeted inhibitors, such as MGCD265, NPS-1034 (*51*), S49076 (*52*), and CEP-40783, that cross-inhibit other RTKs, particularly cMet. Most of these inhibitors are positioned to be used as the second-line treatment after acquiring EGFR resistance (*51*, *53*). However, another potential approach would be to target the mesenchymal system with AXL inhibition as the first-line treatment. This rationale is based on our finding that the RTK activation network exhibit increasingly robust cross-talk along the EMT gradient, thereby drastically sensitizing mesenchymal-like cancer cells to inhibition of the AXL signaling node. Our data also imply that tumors of an epithelial phenotype will also show some sensitivity at higher doses. We speculate that the epithelial cells are likely to retain linear signaling axis, which shows a dose-dependent inhibition. The linear signaling nature of the AXL axis in Epi-A–type tumors has decreased dependency on AXL signaling and suggests that resistance to selective AXL inhibitors would be more likely. It will be worth exploring whether those inhibitors targeting both AXL and other RTKs would be a better choice for the epithelial Epi-A subtype.

There are several strategies to target AXL. Several small–molecular weight compounds that inhibit the kinase pocket of AXL are in the clinical pipelines (*54*). A monoclonal antibody YW327.6S2 has proven to be effective in blocking the GAS6-AXL axis by binding and internalizing AXL (*44*). Apart from targeting AXL directly, a "decoy receptor" has been engineered to bind GAS6 and inhibit its function and has shown to markedly reduce metastatic spread in SKOV3 intraperitoneal mouse model (*55*). Apart from pharmacological inhibition, genetic inhibition of AXL using shRNA showed partial reversal of EMT in ovarian cancer cell lines and reduction in motility and invasion and in tumorigenesis in vivo.

In conclusion, molecular stratification of ovarian cancer by GEMS enables the identification of key players in molecular networks that modulate the functions of a specific molecular subtype, with AXL being a crucial player in the Mes subtype. The GAS6-AXL pathway initiates a recurrent and sustained ERK response exclusively for the Mes subtype, which contributes to an increase in motility and signal amplification via extensive cross-talks with other RTKs. This inherent amplification of oncogenic signaling makes the Mes subtype more sensitive to AXL inhibition. Thus, identifying the Mes-subtype ovarian cancer patients

followed by targeted AXL inhibition would be promising in a prospective clinical setting, such as in platinum-resistant diseases.

MATERIALS AND METHODS

Cell culture

Thirty eight of the 43 SGOCL panel of ovarian cancer cell lines used have been documented previously (*22*). They were cultured in their specified media with requisite amounts of fetal bovine serum and 1% penicillin and streptomycin (Sigma-Aldrich) and grown at 37°C in a 95% air and 5% CO_2–regulated incubator. For kinetic stimulation studies, the 10 epithelial ovarian cancer cell lines were seeded to attain 70% confluence, serum-starved overnight, and activated with GAS6 (400 ng ml^{-1}; #885-GS, R&D Systems) for 0, 10, 20, and 30 min and 1, 3, 6, 12, and 24 hours, and lysates were collected for analysis. For AXL inhibitor studies, the 10 epithelial ovarian cancer cell lines were seeded to obtain 80% confluence at the end of study, incubated with R428 (#BGB324, Selleckchem) at varying doses between 0 and 80 μM for 48 hours to calculate GI_{50} doses. CellTiter MTS cell proliferation assay (#G3580, Promega) was used to evaluate 50% inhibition. For GAS6 kinetics upon AXL inhibition, cells were serum-starved overnight and preincubated with $GI_{50}^{non\text{-}Mes}$ or GI_{50}^{Mes} concentrations of R428 for an hour, whereas control cells were incubated with DMSO and then stimulated with GAS6 (400 ng ml^{-1}) for requisite time points. For the MEK inhibitor studies, cells were preincubated with either no drug (DMSO-only control) or 2 μM PD0325901 for 4 hours and then stimulated with GAS6 to visualize signaling kinetics and motility. For ERK inhibitor studies, cells were preincubated with either DMSO (control) or 5 μM SCH772984 for the required time to study the time course–dependent effects. For transfection experiments in PEO4 and TYKnu cells, IRES-GFP-AXL-KD and pIRESpuro2 AXL were a gift from A. Meyer (plasmids #65498 and #65627, Addgene).

Antibodies

AXL C89E7 rabbit mAb (#8661), phospho-AXL Tyr^{702} D12B2 rabbit mAb (#5724), phospho-AKT Ser^{473} D9E XP rabbit mAb (#4060), phospho-AKT Thr^{308} D25E6 XP rabbit mAb (#13038), AKT pan 11E7 rabbit mAb (#4685), GAPDH D16H11 XP rabbit mAb (#5174), Slug C19G7 rabbit mAb (#9585), phospho-FRA1 Ser^{265} D22B1 rabbit mAb (#5841), phospho-HER2/Erb2 Tyr^{1248} rabbit mAb (#2247), HER2/Erb2 29D8 rabbit mAb (#2165), phospho-EGFR Tyr^{1068} D7A5 XP rabbit mAb (#3777), phospho-Met $Tyr^{1234/1235}$ 3D7 rabbit mAb (#3129), and cMET 25H2 mouse mAb (#3127) were purchased from Cell Signaling Technology (CST). Phospho-ERK1 pT202/pY204 + phospho-ERK2 pT185/pY187 mouse mAb (#ab50011) and ERK1/2 rabbit polyclonal antibody (pAb) (#ab17942) were purchased from Abcam. EGFR/ErbB1 goat pAb (#E1157) was purchased from Sigma-Aldrich. The above listed primary antibodies were used in immunoblotting at 1:1000 dilution. β-Catenin D10A8 XP rabbit mAb (#8480) from CST and E-Cadherin Clone 36/E mouse mAb (#610182) from BD Biosciences were used 1:100 and 1:2000 for immunostaining, respectively. The phospho-HER2, phospho-EGFR, phospho-Met, and AXL antibodies were used at 1:100 for Duolink and immunostaining. The phospho-AXL and phospho-ERK antibodies were used at 1:100 for immunostaining.

Western blotting

Whole-cell lysates were generated by lysis with radioimmunoprecipitation assay (RIPA) buffer (Sigma-Aldrich), along with protease and phosphatase inhibitor cocktails (Calbiochem). Tumor samples from the National University Hospital cohort (GSE69207) that have been previously subtyped (*38*) were lysed in 200 μl of RIPA buffer with protease and phosphatase inhibitor cocktails using a tissue homogenizer. Bicinchoninic acid assay was used to evaluate protein concentrations (#23225, Thermo Scientific). The Bio-Rad Mini Protean II apparatus was used to perform gel electrophoresis on the lysates, and the Bio-Rad Mini Trans-Blot apparatus was used to transfer the gel onto polyvinylidene difluoride membranes (#IPFL00010, Millipore). Membranes were blocked with LI-COR blocking buffer (#927-40000) and subsequently probed with primary antibodies. Incubation with secondary antibodies containing fluorophores at 1:20,000 dilution [IRDye 800CW–conjugated goat anti-rabbit (#926-32211) and IRDye 680–conjugated goat anti-mouse antibodies (#926-32220), LI-COR Biosciences] enabled visualization on the Odyssey Infrared Imaging System from LI-COR Biosciences. Full-length blots for the various experiments are shown in fig. S8.

Single-cell motility tracking

The 10 epithelial ovarian cancer cell lines were seeded at 50% confluence in ibidi 24-well microplate and serum-starved overnight. They were stained for an hour with Hoechst nuclear dye (1:500,000; #62249, Life Technologies) and then stimulated with GAS6 (400 ng ml^{-1}), whereas control cells were left untreated and visualized under the SP5 Leica Confocal system overnight at intervals of 10 min. The results were analyzed in ImageJ software using TrackMate to calculate individual cellular displacements, velocity of locomotion, speed, distance travelled, and directional persistence. In the R428 studies, the cells were serum-starved overnight and preincubated with $GI_{50}^{non\text{-}Mes}$ or GI_{50}^{Mes} concentrations of R428 for an hour, whereas control cells were incubated with DMSO and then stimulated with GAS6 (400 ng ml^{-1}).

Gap closure assays

The 10 epithelial ovarian cancer cell lines were seeded at 100% confluence into culture inserts (#80209, ibidi) in a 24-well microplate and serum-starved overnight. CellMask membrane dye (1:4000; #C10049, Life Technologies) was added for an hour, the insert was removed to generate a 500-μm gap and stimulated with GAS6 (400 ng ml^{-1}). Control cells were not stimulated. The cells were visualized under the SP5 Leica Confocal system overnight at intervals of 10 min. The results were analyzed in ImageJ software to generate the gap closure at 12 hours after GAS6 stimulation.

Reverse-phase protein array

Mes-subtype SKOV3 cell line and Epi-A subtype PEO1 cell line were serum-starved overnight and treated with GAS6 (400 ng ml^{-1}) for 30 min or 12 hours, whereas control cells were untreated. RPPA procedure involved serial dilution of samples and subsequent colorimetric detection by antibodies upon tyramid amplification. Spot intensity assessment was done using the R package developed in-house at the MD Anderson Cancer Center with protein levels quantified by SuperCurve method (http://bioinformatics.mdanderson.org/OOMPA). Data were log-transformed (base 2) and median-control–normalized across all proteins within a sample. The RPPA antibody list can be obtained at www.mdanderson.org/education-and-research/resources-for-professionals/scientific-resources/core-facilities-and-services/functional-proteomics-rppa-core/antibody-lists-protocols/functional-proteomics-reverse-phase-protein-array-core-facility-antibody-lists-and-protocols.html.

Also, for the abundance of pMAPK ($pThr^{202}$) in ovarian tumors, level 3 RPPA data of ovarian cancer clinical samples were downloaded from TCGA data portal (https://tcga-data.nci.nih.gov/tcga/). The subtype information was extracted from our previous gene expression analysis of the corresponding samples (*3*).

Duolink PLA assay

For this proximity ligation amplification (PLA) assay (#DUO92102 and #DUO92104, Duolink, OLink Biosceinces, Sigma-Aldrich), cells were seeded on glass coverslips, serum-starved overnight, and treated with GAS6 (400 ng ml^{-1}) for 30 min; control cells were untreated. The manufacturer's instructions were followed.

Immunofluorescence staining

Cells were seeded on coverslips in full medium and left to adhere for 24 hours and to reach 50% confluence. After necessary serum depletion and/or treatments, cells were fixed with ice-cold 100% methanol for 5 min at −20°C and then rehydrated thrice in phosphate-buffered saline (PBS) for 5 min each. Coverslips were blocked for 30 min with 3% bovine serum albumin (BSA)/PBS and then incubated with primary antibodies in 1% BSA/PBS for 1 hour in a moist environment. After three washes with PBS, cells were incubated with fluorescently labeled secondary antibodies (1:400; Alexa Fluor Life Technologies, donkey anti-mouse, donkey anti-goat or donkey anti-mouse) in 1% BSA/PBS for 1 hour. After three washes with PBS, the coverslips were mounted using ProLong Gold antifade with 4′,6-diamidino-2-phenylindole (DAPI) with mounting medium.

Cholesterol depletion protocol

MBCD (#C4555, Sigma-Aldrich) was used to deplete cholesterol. PEO1, OVCA429, SKOV3, and HEYA8 cells were grown on 13-mm coverslips and treated with 5 mM MBCD for 30 min at 37°C; control cells were maintained without cholesterol depletion. After MBCD treatment, cells were allowed to recover for 0 and 30 min, and 12 hours in serum-free medium and then fixed with ice-cold methanol for 5 min and rehydrated thrice with PBS. The cells were stained with Filipin (0.05 mg ml^{-1}; #C4767, Sigma-Aldrich), diluted in PBS for 1 hour at room temperature, and rinsed thrice with PBS. The coverslips were mounted in non-DAPI mounting medium, and the filipin staining was observed under the 405-nm wavelength of a fluorescent microscope.

Chick CAM model

Fertilized chicken eggs were purchased from Henry Stewart & Co. Ltd., washed, and incubated at 37°C with 60% relative humidity on embryonic day 1 (ED1), for implantation on ED4. The method for the preparation of the CAM was a modification of a previously described technique (*56*). Under sterile conditions, a small hole was pierced through the pointed pole of the shell using a 19-gauge needle, and a 2-cm diameter window of shell was removed to expose the CAM. The inner shell membrane was carefully removed with sterile forceps to expose the CAM. This window was covered with a sterile 10-mm tissue culture dish and sealed with Suprasorb F sterile wound healing film (Lohmann & Rauscher). Between ED7 and ED10 of incubation, the membranes are ready for the grafting of cancer cells. PEO1, OVCA429, SKOV3, and HEYA8 cells were preincubated with DMSO only (control cells) or with $GI_{50}^{non\text{-}Mes}$ or GI_{50}^{Mes} concentrations of R428 for 48 hours. Grafts were prepared by suspending 10^6 cells in 100 µl of Matrigel (BD Biosciences). A medium to large blood vessel was then bruised using a sterile cotton bud, and 25 µl of the prepared graft, containing 1×10^6 cells was then inoculated onto this area. After inoculation, the window was covered, sealed, and placed back in the incubator. Tumor growth and viability of the embryo were checked daily. Tumor dimensions were measured using SteREO Discovery.V8 microscope (Zeiss) with the Zen 2.0 blue edition software (Zeiss).

AXL knockdown

Five validated AXL MISSION shRNA and control shRNA (shLuciferase targeting) bacterial glycerol stocks were purchased from Sigma-Aldrich. DNA was purified and extracted using PureYield Plasmid Miniprep System (Promega) and used to transfect 293T cells according to the manufacturer's protocol. The virus generated was subsequently filtered to remove 293T cell debris and used to infect OVCA429 and SKOV3 with polybrene (4 µg ml^{-1}). The sequences that gave the maximum decrease in AXL protein abundance after infection and selection with puromycin (5 µg ml^{-1}) were the following: TRCN0000001040 (clone ID, NM_021913.x-2909s1c1; sequence, *CCGGCGAAATCCTCTATGTCAACATCTCGAGATGTTGACATAGAGGATTTCGTTTTT*) and TRCN0000001041 (clone ID, NM_021913.x-2151s1c1; sequence, *CCGGGCTGTGAAGACGATGAAGATTCTCGAGAATCTTCATCGTCTTCACAGCTTTTT*). The nonspecific shLuciferase had the sequence *CCGGCGCTGAGTACTTCGAAATGTCCTCGAGGACATTTCGAAGTACTCAGCGTTTTT* (#SHC007). For the single-cell motility and gap closure assays, cells were seeded in complete medium and the experiments were carried out as described.

Soft agar assay

Cells (10^6) from shAXL clones and control of SKOV3 and OVCA429 were seeded in a six-well plate using a previously established protocol. The anoikis-resistant cells formed colonies on the soft agar and were visualized on day 14.

Spheroid invasion assay

Cells (5000) from shAXL clones and control of SKOV3 and OVCA429 were seeded in a Cultrex 96-well kit (3-D Spheroid BME Cell Invasion Assay; #3500-096-K, Trevigen), and the assay was performed following the manufacturer's protocol. Cell invasion was monitored over time, and optimal results were documents on day 3.

SKOV3 orthotopic xenograft mouse model

The SKOV3 orthotopic xenograft model was established by GenScript. The procedures involving the care and use of animals were reviewed and approved by the Institutional Animal Care and Use Committee to ensure compliance with the regulations of the Association for Assessment and Accreditation of Laboratory Animal Care. Five 6-week-old female SCID-Beige mice were used per condition and inoculated by intraperitoneal injection with a single volume of 200 µl of cell suspension with 5×10^6 cells to establish SKOV3 shLuciferase control, shAXL#40, and shAXL#41 ovarian cancer models. The study was concluded 4 weeks after injection of cells, and the number of tumors and tumor mass was assessed in each mouse using calibrated calipers. Tumor volume was calculated using the formula $\text{width}^2 \times \text{length} \times 0.5$.

Gene expression analysis and *AXL* signature

Gene expression data were extracted from previously processed meta-analysis of 1538 ovarian cancer (*3*). To derive the AXL signature, genes that are most strongly and positively correlated with *AXL* gene expression (Rho > +0.45) were selected.

Statistical analysis

Statistical analyses were conducted using MATLAB R2012a version 7.14.0.739 and statistics toolbox version 8.0 (MathWorks). Statistical significance of differential expression was evaluated using either Student's *t* test or Mann-Whitney *U* test. A Spearman correlation coefficient test was applied to assess significance of correlation. Kaplan-Meier analyses

were conducted using GraphPad Prism version 5.04 (GraphPad Software). Statistical significance of the Kaplan-Meier analysis was calculated by log-rank test. To perform Kaplan-Meier analysis of overall and disease-free survival for AXL signature in various cancers, stratification of patients was based on AXL signature score, which segregates patients into AXL-high and AXL-low groups referring to median score, or AXL-Q1 and AXL-Q4 referring to lowest 25% and highest 25% signature scores, respectively.

SUPPLEMENTARY MATERIALS

www.sciencesignaling.org/cgi/content/full/9/448/ra97/DC1

Fig. S1. *AXL* rank and expression in GEMS and EMT phenotype.

Fig. S2. AXL signaling in GEMS has divergent biological consequences.

Fig. S3. GAS6-AXL signaling relies on MEK-ERK pathway to promote motility in Mes-subtype tumor cells.

Fig. S4. Epi-A cells show membrane modulation of AXL-RTK networks and DUSP4 regulation of the pERK response.

Fig. S5. Mes- subtype cells are more sensitive to AXL-specific inhibition.

Fig. S6. AXL mediates the phenotypic transitions of EMT.

Fig. S7. The AXL gene signature is enriched in Mes-subtype tumors and correlates with worse prognosis in patients.

Fig. S8. Full-length blots.

Table S1. High *AXL* expression predicts poor prognosis in ovarian cancer in multivariate analysis.

Table S2. High *AXL* expression predicts poor prognosis in ovarian cancer even when accounting for the effect arising from the GEMS.

Table S3. The AXL gene signature is prognostically relevant in ovarian cancer.

REFERENCES AND NOTES

1. R. W. Tothill, A. V. Tinker, J. George, R. Brown, S. B. Fox, S. Lade, D. S. Johnson, M. K. Trivett, D. Etemadmoghadam, B. Locandro, N. Traficante, S. Fereday, J. A. Hung, Y.-E. Chiew, I. Haviv; Australian Ovarian Cancer Study Group, D. Gertig, A. deFazio, D. D. L. Bowtell, Novel molecular subtypes of serous and endometrioid ovarian cancer linked to clinical outcome. *Clin. Cancer Res.* **14**, 5198–5208 (2008).
2. Cancer Genome Atlas Research Network, Integrated genomic analyses of ovarian carcinoma. *Nature* **474**, 609–615 (2011).
3. T. Z. Tan, Q. H. Miow, R. Y.-J. Huang, M. K. Wong, J. Ye, J. A. Lau, M. C. Wu, L. H. Bin Abdul Hadi, R. Soong, M. Choolani, B. Davidson, J. M. Nesland, L.-Z. Wang, N. Matsumura, M. Mandai, I. Konishi, B.-C. Goh, J. T. Chang, J. P. Thiery, S. Mori, Functional genomics identifies five distinct molecular subtypes with clinical relevance and pathways for growth control in epithelial ovarian cancer. *EMBO Mol. Med.* **5**, 983–998 (2013).
4. A. Helland, M. S. Anglesio, J. George, P. A. Cowin, C. N. Johnstone, C. M. House, K. E. Sheppard, D. Etemadmoghadam, N. Melnyk, A. K. Rustgi, W. A. Phillips, H. Johnsen, R. Holm, G. B. Kristensen, M. J. Birrer; Australian Ovarian Cancer Study Group, R. B. Pearson, A.-L. Børresen-Dale, D. G. Huntsman, A. deFazio, C. J. Creighton, G. K. Smyth, D. D. L. Bowtell, Deregulation of *MYCN*, *LIN28B* and *LET7* in a molecular subtype of aggressive high-grade serous ovarian cancers. *PLOS ONE* **6**, e18064 (2011).
5. M. Asad, M. K. Wong, T. Z. Tan, M. Choolani, J. Low, S. Mori, D. Virshup, J. P. Thiery, R. Y.-J. Huang, *FZD7* drives in vitro aggressiveness in Stem-A subtype of ovarian cancer via regulation of non-canonical Wnt/PCP pathway. *Cell Death Dis.* **5**, e1346 (2014).
6. J. P. Thiery, H. Acloque, R. Y. J. Huang, M. A. Nieto, Epithelial-mesenchymal transitions in development and disease. *Cell* **139**, 871–890 (2009).
7. V. Y. Chung, T. Z. Tan, M. Tan, M. K. Wong, K. T. Kuay, Z. Yang, J. Ye, J. Muller, C. M. Koh, E. Guccione, J. P. Thiery, R. Y.-J. Huang, GRHL2-miR-200-ZEB1 maintains the epithelial status of ovarian cancer through transcriptional regulation and histone modification. *Sci. Rep.* **6**, 19943 (2016).
8. R. M. A. Linger, A. K. Keating, H. S. Earp, D. K. Graham, TAM receptor tyrosine kinases: Biologic functions, signaling, and potential therapeutic targeting in human cancer. *Adv. Cancer Res.* **100**, 35–83 (2008).
9. S. Goruppi, E. Ruaro, C. Schneider, Gas6, the ligand of Axl tyrosine kinase receptor, has mitogenic and survival activities for serum starved NIH3T3 fibroblasts. *Oncogene* **12**, 471–480 (1996).
10. C. Gjerdrum, C. Tiron, T. Høiby, I. Stefansson, H. Haugen, T. Sandal, K. Collett, S. Li, E. McCormack, B. T. Gjertsen, D. R. Micklem, L. A. Akslen, C. Glackin, J. B. Lorens, Axl is an essential epithelial-to-mesenchymal transition-induced regulator of breast cancer metastasis and patient survival. *Proc. Natl. Acad. Sci. U.S.A.* **107**, 1124–1129 (2010).
11. M. Ishikawa, M. Sonobe, E. Nakayama, M. Kobayashi, R. Kikuchi, J. Kitamura, N. Imamura, H. Date, Higher expression of receptor tyrosine kinase Axl, and differential expression of its ligand, Gas6, predict poor survival in lung adenocarcinoma patients. *Ann. Surg. Oncol.* **20** (Suppl. 3), S467–S476 (2013).
12. S. J. Holland, A. Pan, C. Franci, Y. Hu, B. Chang, W. Li, M. Duan, A. Torneros, J. Yu, T. J. Heckrodt, J. Zhang, P. Ding, A. Apatira, J. Chua, R. Brandt, P. Pine, D. Goff, R. Singh, D. G. Payan, Y. Hitoshi, R428, a selective small molecule inhibitor of Axl kinase, blocks tumor spread and prolongs survival in models of metastatic breast cancer. *Cancer Res.* **70**, 1544–1554 (2010).
13. X. Song, H. Wang, C. D. Logsdon, A. Rashid, J. B. Fleming, J. L. Abbruzzese, H. F. Gomez, D. B. Evans, H. Wang, Overexpression of receptor tyrosine kinase Axl promotes tumor cell invasion and survival in pancreatic ductal adenocarcinoma. *Cancer* **117**, 734–743 (2011).
14. Z. Zhang, J. C. Lee, L. Lin, V. Olivas, V. Au, T. LaFramboise, M. Abdel-Rahman, X. Wang, A. D. Levine, J. K. Rho, Y. J. Choi, C.-M. Choi, S.-W. Kim, S. J. Jang, Y. S. Park, W. S. Kim, D. H. Lee, J.-S. Lee, V. A. Miller, M. Arcila, M. Ladanyi, P. Moonsamy, C. Sawyers, T. J. Boggon, P. C. Ma, C. Costa, M. Taron, R. Rosell, B. Halmos, T. G. Bivona, Activation of the AXL kinase causes resistance to EGFR-targeted therapy in lung cancer. *Nat. Genet.* **44**, 852–860 (2012).
15. L. A. Byers, L. Diao, J. Wang, P. Saintigny, L. Girard, M. Peyton, L. Shen, Y. Fan, U. Giri, P. K. Tumula, M. B. Nilsson, J. Gudikote, H. Tran, R. J. G. Cardnell, D. J. Bearss, S. L. Warner, J. M. Foulks, S. B. Kanner, V. Gandhi, N. Krett, S. T. Rosen, E. S. Kim, R. S. Herbst, G. R. Blumenschein, J. J. Lee, S. M. Lippman, K. K. Ang, G. B. Mills, W. K. Hong, J. N. Weinstein, I. I. Wistuba, K. R. Coombes, J. D. Minna, J. V. Heymach, An epithelial–mesenchymal transition gene signature predicts resistance to EGFR and PI3K inhibitors and identifies Axl as a therapeutic target for overcoming EGFR inhibitor resistance. *Clin. Cancer Res.* **19**, 279–290 (2013).
16. M. Elkabets, E. Pazarentzos, D. Juric, Q. Sheng, R. A. Pelossof, S. Brook, A. O. Benzaken, J. Rodon, N. Morse, J. J. Yan, M. Liu, R. Das, Y. Chen, A. Tam, H. Wang, J. Liang, J. M. Gurski, D. A. Kerr, R. Rosell, C. Teixidó, A. Huang, R. A. Ghossein, N. Rosen, T. G. Bivona, M. Scaltriti, J. Baselga, AXL mediates resistance to PI3Kα inhibition by activating the EGFR/PKC/mTOR axis in head and neck and esophageal squamous cell carcinomas. *Cancer Cell* **27**, 533–546 (2015).
17. D. K. Graham, D. DeRyckere, K. D. Davies, H. S. Earp, The TAM family: Phosphatidylserine-sensing receptor tyrosine kinases gone awry in cancer. *Nat. Rev. Cancer* **14**, 769–785 (2014).
18. E. B. Rankin, K. C. Fuh, T. E. Taylor, A. J. Krieg, M. Musser, J. Yuan, K. Wei, C. J. Kuo, T. A. Longacre, A. J. Giaccia, AXL is an essential factor and therapeutic target for metastatic ovarian cancer. *Cancer Res.* **70**, 7570–7579 (2010).
19. C. Sotiriou, L. Pusztai, Gene-expression signatures in breast cancer. *N. Engl. J. Med.* **360**, 790–800 (2009).
20. D. Yang, Y. Sun, L. Hu, H. Zheng, P. Ji, C. V. Pecot, Y. Zhao, S. Reynolds, H. Cheng, R. Rupaimoole, D. Cogdell, M. Nykter, R. Broaddus, C. Rodriguez-Aguayo, G. Lopez-Berestein, J. Liu, I. Shmulevich, A. K. Sood, K. Chen, W. Zhang, Integrated analyses identify a master microRNA regulatory network for the mesenchymal subtype in serous ovarian cancer. *Cancer Cell* **23**, 186–199 (2013).
21. H. S. Leong, L. Galletta, D. Etemadmoghadam, J. George; Australian Ovarian Cancer Study, M. Köbel, S. J. Ramus, D. Bowtell, Efficient molecular subtype classification of high-grade serous ovarian cancer. *J. Pathol.* **236**, 272–277 (2015).
22. R. Y.-J. Huang, M. K. Wong, T. Z. Tan, K. T. Kuay, A. H. C. Ng, V. Y. Chung, Y.-S. Chu, N. Matsumura, H.-C. Lai, Y. F. Lee, W.-J. Sim, C. Chai, E. Pietschmann, S. Mori, J. J. H. Low, M. Choolani, J. P. Thiery, An EMT spectrum defines an anoikis-resistant and spheroidogenic intermediate mesenchymal state that is sensitive to e-cadherin restoration by a src-kinase inhibitor, saracatinib (AZD0530). *Cell Death Dis.* **4**, e915 (2013).
23. C. J. Marshall, Specificity of receptor tyrosine kinase signaling: Transient versus sustained extracellular signal-regulated kinase activation. *Cell* **80**, 179–185 (1995).
24. B. N. Kholodenko, J. F. Hancock, W. Kolch, Signalling ballet in space and time. *Nat. Rev. Mol. Cell Biol.* **11**, 414–426 (2010).
25. T. Sawabu, H. Seno, T. Kawashima, A. Fukuda, Y. Uenoyama, M. Kawada, N. Kanda, A. Sekikawa, H. Fukui, M. Yanagita, H. Yoshibayashi, S. Satoh, Y. Sakai, T. Nakano, T. Chiba, Growth arrest-specific gene 6 and Axl signaling enhances gastric cancer cell survival via Akt pathway. *Mol. Carcinog.* **46**, 155–164 (2007).
26. K. Rea, P. Pinciroli, M. Sensi, F. Alciato, B. Bisaro, L. Lozneanu, F. Raspagliesi, F. Centritto, S. Cabodi, P. Defilippi, G. C. Avanzi, S. Canevari, A. Tomassetti, Novel Axl-driven signaling pathway and molecular signature characterize high-grade ovarian cancer patients with poor clinical outcome. *Oncotarget* **6**, 30859–30875 (2015).
27. E. Vial, C. J. Marshall, Elevated ERK-MAP kinase activity protects the FOS family member FRA-1 against proteasomal degradation in colon carcinoma cells. *J. Cell Sci.* **116**, 4957–4963 (2003).

28. L. Bakiri, S. Macho-Maschler, I. Custic, J. Niemiec, A. Guío-Carrión, S. C. Hasenfuss, A. Eger, M. Müller, H. Beug, E. F. Wagner, Fra-1/AP-1 induces EMT in mammary epithelial cells by modulating Zeb1/2 and TGFβ expression. *Cell Death Differ.* **22**, 336–350 (2015).
29. K.-N. Chua, W.-J. Sim, V. Racine, S.-Y. Lee, B. C. Goh, J. P. Thiery, A cell-based small molecule screening method for identifying inhibitors of epithelial-mesenchymal transition in carcinoma. *PLOS ONE* **7**, e33183 (2012).
30. E. J. Morris, S. Jha, C. R. Restaino, P. Dayananth, H. Zhu, A. Cooper, D. Carr, Y. Deng, W. Jin, S. Black, B. Long, J. Liu, E. Dinunzio, W. Windsor, R. Zhang, S. Zhao, M. H. Angagaw, E. M. Pinheiro, J. Desai, L. Xiao, G. Shipps, A. Hruza, J. Wang, J. Kelly, S. Paliwal, X. Gao, B. S. Babu, L. Zhu, P. Daublain, L. Zhang, B. A. Lutterbach, M. R. Pelletier, U. Philippar, P. Siliphaivanh, D. Witter, P. Kirschmeier, W. R. Bishop, D. Hicklin, D. G. Gilliland, L. Jayaraman, L. Zawel, S. Fawell, A. A. Samatar, Discovery of a novel ERK inhibitor with activity in models of acquired resistance to BRAF and MEK inhibitors. *Cancer Discov.* **3**, 742–750 (2013).
31. J. Yang, S. A. Mani, J. L. Donaher, S. Ramaswamy, R. A. Itzykson, C. Come, P. Savagner, I. Gitelman, A. Richardson, R. A. Weinberg, Twist, a master regulator of morphogenesis, plays an essential role in tumor metastasis. *Cell* **117**, 927–939 (2004).
32. A. S. Meyer, A. J. M. Zweemer, D. A. Lauffenburger, The AXL receptor is a sensor of ligand spatial heterogeneity. *Cell Syst.* **1**, 25–36 (2015).
33. K. Simons, E. Ikonen, Functional rafts in cell membranes. *Nature* **387**, 569–572 (1997).
34. N. L. G. Sieben, J. Oosting, A. M. Flanagan, J. Prat, G. M. J. M. Roemen, S. M. Kolkman-Uljee, R. van Eijk, C. J. Cornelisse, G. J. Fleuren, M. van Engeland, Differential gene expression in ovarian tumors reveals *Dusp 4* and *Serpina 5* as key regulators for benign behavior of serous borderline tumors. *J. Clin. Oncol.* **23**, 7257–7264 (2005).
35. T. Z. Tan, Q. H. Miow, Y. Miki, T. Noda, S. Mori, R. Y.-J. Huang, J. P. Thiery, Epithelial-mesenchymal transition spectrum quantification and its efficacy in deciphering survival and drug responses of cancer patients. *EMBO Mol. Med.* **6**, 1279–1293 (2014).
36. A. S. Brodsky, A. Fischer, D. H. Miller, S. Vang, S. MacLaughlan, H.-T. Wu, J. Yu, M. Steinhoff, C. Collins, P. J. S. Smith, B. J. Raphael, L. Brard, Expression profiling of primary and metastatic ovarian tumors reveals differences indicative of aggressive disease. *PLOS ONE* **9**, e94476 (2014).
37. S. Marchini, R. Fruscio, L. Clivio, L. Beltrame, L. Porcu, I. Fuso Nerini, D. Cavalieri, G. Chiorino, G. Cattoretti, C. Mangioni, R. Milani, V. Torri, C. Romualdi, A. Zambelli, M. Romano, M. Signorelli, S. di Giandomenico, M. D'Incalci, Resistance to platinum-based chemotherapy is associated with epithelial to mesenchymal transition in epithelial ovarian cancer. *Eur. J. Cancer* **49**, 520–530 (2013).
38. T. Z. Tan, H. Yang, J. Ye, J. Low, M. Choolani, D. S. P. Tan, J.-P. Thiery, R. Y.-J. Huang, CSIOVDB: A microarray gene expression database of epithelial ovarian cancer subtype. *Oncotarget* **6**, 43843–43852 (2015).
39. J. P. O'Bryan, R. A. Frye, P. C. Cogswell, A. Neubauer, B. Kitch, C. Prokop, R. Espinosa III, M. M. Le Beau, H. S. Earp, E. T. Liu, *axl*, a transforming gene isolated from primary human myeloid leukemia cells, encodes a novel receptor tyrosine kinase. *Mol. Cell. Biol.* **11**, 5016–5031 (1991).
40. T. S. Gujral, R. L. Karp, A. Finski, M. Chan, P. E. Schwartz, G. MacBeath, P. Sorger, Profiling phospho-signaling networks in breast cancer using reverse-phase protein arrays. *Oncogene* **32**, 3470–3476 (2013).
41. L. Liu, J. Greger, H. Shi, Y. Liu, J. Greshock, R. Annan, W. Halsey, G. M. Sathe, A.-M. Martin, T. M. Gilmer, Novel mechanism of lapatinib resistance in HER2-positive breast tumor cells: Activation of AXL. *Cancer Res.* **69**, 6871–6878 (2009).
42. A. S. Meyer, M. A. Miller, F. B. Gertler, D. A. Lauffenburger, The receptor AXL diversifies EGFR signaling and limits the response to EGFR-targeted inhibitors in triple-negative breast cancer cells. *Sci. Signal.* **6**, ra66 (2013).
43. L. Cerchia, C. L. Esposito, S. Camorani, A. Rienzo, L. Stasio, L. Insabato, A. Affuso, V. de Franciscis, Targeting Axl with an high-affinity inhibitory aptamer. *Mol. Ther.* **20**, 2291–2303 (2012).
44. X. Ye, Y. Li, S. Stawicki, S. Couto, J. Eastham-Anderson, D. Kallop, R. Weimer, Y. Wu, L. Pei, An anti-Axl monoclonal antibody attenuates xenograft tumor growth and enhances the effect of multiple anticancer therapies. *Oncogene* **29**, 5254–5264 (2010).
45. W. Leconet, C. Larbouret, T. Chardès, G. Thomas, M. Neiveyans, M. Busson, M. Jarlier, N. Radosevic-Robin, M. Pugnière, F. Bernex, F. Penault-Llorca, J.-M. Pasquet, A. Pèlegrin, B. Robert, Preclinical validation of AXL receptor as a target for antibody-based pancreatic cancer immunotherapy. *Oncogene* **33**, 5405–5414 (2014).
46. E. Vial, E. Sahai, C. J. Marshall, ERK-MAPK signaling coordinately regulates activity of Rac1 and RhoA for tumor cell motility. *Cancer Cell* **4**, 67–79 (2003).
47. H.-J. Lee, Y.-M. Jeng, Y.-L. Chen, L. Chung, R.-H. Yuan, Gas6/Axl pathway promotes tumor invasion through the transcriptional activation of Slug in hepatocellular carcinoma. *Carcinogenesis* **35**, 769–775 (2014).
48. S. Shin, J. Blenis, ERK2/Fra1/ZEB pathway induces epithelial-to-mesenchymal transition. *Cell Cycle* **9**, 2483–2484 (2010).
49. C. Wilson, X. Ye, T. Pham, E. Lin, S. Chan, E. McNamara, R. M. Neve, L. Belmont, H. Koeppen, R. L. Yauch, A. Ashkenazi, J. Settleman, AXL inhibition sensitizes mesenchymal cancer cells to antimitotic drugs. *Cancer Res.* **74**, 5878–5890 (2014).
50. F. Wu, J. Li, C. Jang, J. Wang, J. Xiong, The role of Axl in drug resistance and epithelial-to-mesenchymal transition of non-small cell lung carcinoma. *Int. J. Clin. Exp. Pathol.* **7**, 6653–6661 (2014).
51. J. K. Rho, Y. J. Choi, S. Y. Kim, T. W. Kim, E. K. Choi, S.-J. Yoon, B. M. Park, E. Park, J. H. Bae, C.-M. Choi, J. C. Lee, MET and AXL inhibitor NPS-1034 exerts efficacy against lung cancer cells resistant to EGFR kinase inhibitors because of MET or AXL activation. *Cancer Res.* **74**, 253–262 (2014).
52. M. F. Burbridge, C. J. Bossard, C. Saunier, I. Fejes, A. Bruno, S. Léonce, G. Ferry, G. Da Violante, F. Bouzom, V. Cattan, A. Jacquet-Bescond, P. M. Comoglio, B. P. Lockhart, J. A. Boutin, A. Cordi, J.-C. Ortuno, A. Pierré, J. A. Hickman, F. H. Cruzalegui, S. Depil, S49076 is a novel kinase inhibitor of MET, AXL, and FGFR with strong preclinical activity alone and in association with bevacizumab. *Mol. Cancer Ther.* **12**, 1749–1762 (2013).
53. X. Wu, X. Liu, S. Koul, C. Y. Lee, Z. Zhang, B. Halmos, AXL kinase as a novel target for cancer therapy. *Oncotarget* **5**, 9546–9563 (2014).
54. R. A. Okimoto, T. G. Bivona, AXL receptor tyrosine kinase as a therapeutic target in NSCLC. *Lung Cancer Targets and Ther.* **2015**, 27–34 (2015).
55. M. S. Kariolis, Y. R. Miao, D. S. Jones II, S. Kapur, I. I. Mathews, A. J. Giaccia, J. R. Cochran, An engineered Axl 'decoy receptor' effectively silences the Gas6-Axl signaling axis. *Nat. Chem. Biol.* **10**, 977–983 (2014).
56. D. H. Ausprunk, D. R. Knighton, J. Folkman, Vascularization of normal and neoplastic tissues grafted to the chick chorioallantois. Role of host and preexisting graft blood vessels. *Am. J. Pathol.* **79**, 597–618 (1975).

Funding: This work was supported by the National Research Foundation Singapore and the Singapore Ministry of Education under its Research Centres of Excellence initiative to J.P.T., and the National Medical Research Council under its Centre Grant scheme to the National University Cancer Institute under the EMT Theme to J.P.T. and R.Y.-J.H. **Author contributions:** H.G., C.R., J.P.T., and R.Y.-J.H. devised the project, and H.G., J.P.T., and R.Y.-J.H. obtained funding; J.A., T.Z.T., C.R., and R.Y.-J.H. wrote the paper; J.A. performed all the experiments; T.Z.T. performed bioinformatics analyses; Z.K. performed the CAM assays; and J.L. and M.C. provided clinical samples. **Competing interests:** The authors declare that they have no competing interests.

Submitted 4 April 2016
Accepted 13 September 2016
Published 4 October 2016
10.1126/scisignal.aaf8175

Citation: J. Antony, T. Z. Tan, Z. Kelly, J. Low, M. Choolani, C. Recchi, H. Gabra, J. P. Thiery, R. Y.-J. Huang, The GAS6-AXL signaling network is a mesenchymal (Mes) molecular subtype–specific therapeutic target for ovarian cancer. *Sci. Signal.* **9**, ra97 (2016).

The GAS6-AXL signaling network is a mesenchymal (Mes) molecular subtype–specific therapeutic target for ovarian cancer

Jane Antony, Tuan Zea Tan, Zoe Kelly, Jeffrey Low, Mahesh Choolani, Chiara Recchi, Hani Gabra, Jean Paul Thiery and Ruby Yun-Ju Huang (October 4, 2016)

Science Signaling **9** (448), ra97. [doi: 10.1126/scisignal.aaf8175]